buildings

MDPI

Article

FRP Cables to Prestress RC Beams: State of the Art vs. a Split Wedge Anchorage System

Marco Damiani, Attilio Quadrino and Nicola Nisticò *

Department of Structural and Geotechnical Engineering, Sapienza University of Rome, Via Eudossiana 18, 00184 Rome, Italy; marco.damiani@uniroma1.it (M.D.); attilio.quadrino@uniroma1.it (A.Q.)
* Correspondence: nicola.nistico@uniroma1.it

Abstract: Versatility and high performance in terms of specific stiffness and strength, as well as non-corrosive sensitivity, make FRP (Fiber-Reinforced Polymer) cables a viable alternative to steel ones in the development of prestressing systems. On the other hand, the orthotropic and brittle nature of FRPs could trigger a premature failure of the cable in the anchorage system, for which several solutions have been proposed so far in civil structural applications. In this context, after a preliminary state of the art, the work introduces a split wedge anchorage for FRP (ϕ = 12 mm) cables proposing two different solutions for steel wedges having the external surface: either (1) a constant (3 degrees) slope or (2) a double slope obtained by shaping it with an angle of 3.0 degrees before and then of 3.1 degrees along the most tapered part. The goal was to exploit the nominal cable capacity (257 kN), avoiding stress peaks that cause its premature failure. The proposed solutions have been experimentally tested and, as far as the double angle solution is concerned, the failure loads were equal to 222 and 257 kN, denoting that the proposed solution can reach the cable capacity. Clearly, further investigations are needed to check the variability of the results and eventually improve the system.

Keywords: prestressing system; FRP cables; split wedge anchorage system; experimental tests

Citation: Damiani, M.; Quadrino, A.; Nisticò, N. FRP Cables to Prestress RC Beams: State of the Art vs. a Split Wedge Anchorage System. *Buildings* **2021**, *11*, 209. https://doi.org/10.3390/buildings11050209

Academic Editors: Alessandra Aprile, Giorgio Monti and Eva O.L. Lantsoght

Received: 23 March 2021
Accepted: 14 May 2021
Published: 17 May 2021

1. Introduction

Italian existing infrastructures include reinforced concrete bridges that mainly date back to the 1960s. Over the years, the degradation of material occurs as well as more demanding design rules, so that structural ameliorations could be needed. In the past, FRPs were introduced as advanced materials for the renewal of civil infrastructures [1], which is mainly due to high environmental resistance, stiffness, and strength-to-weight ratios, if compared to traditionally adopted materials such as concrete and steel.

As far as their application in new civil construction is concerned, the idea of replacing steel rods and strands with FRPs was introduced during the 1990s, starting from USA [2] and Japanese [3] recommendations. Applications of FRP materials in bridges are traced in the research of Bank (2006) [4]: FRP elements have been adopted to realize (1) pedestrian bridge parts as well as (2) highway bridge decks and girders. Applications in civil engineering are also discussed in [5–7].

Proposals for the use of FRP cables to prestress reinforced concrete beams date back to the 1980s. Burgoyne (1987) [8] proposed the use of Parafil® Aramid ropes as a prestressing external system, in order to increase the capacity of bridge beams. Those ropes were adopted to support the bridge deck of the Aberfeldy footbridge [9], which was entirely made of FRP elements. The main advantages, if compared with steel cables, are (1) the environmental resistance, including the absence of corrosion, and (2) the lightness, which simplifies their installation in places that are difficult to access.

When FRP cables are used either for prestressing structural elements or supporting bridge decks, their anchorages need to be properly designed to reduce the cable stress state. Different types of anchorage systems have been proposed in technical and scientific

literature so far, and a state of the art review is reported in different works [10–15]. These systems include bonded and mechanical devices.

Bonded anchorages have been discussed in Puigvert et al. (2014), where the authors analyzed static [16], fatigue, and creep [17], as well as the stress relaxation behavior [18] of pultruded FRP carbon cables glued with epoxy resin into steel tubes of different size. An innovative solution to reduce the stress concentration has been introduced by the patent of Meier et al. (1998) [19]: the authors proposed a conical anchor system filled with a gradient material, whose stiffness decreases where bonding stress tends to be greater.

Mechanical devices include clamping, spike, and split wedge systems. In clamping anchorages, one or more bars are arranged between two steel plates, which are then joined by tightening steel bolts. Spike systems basically consist of a conical plug, the spike, and a steel socket. The earliest spike systems date back to the 1970s, when Davis (1972) patented [20] an anchorage made of an external barrel containing a fiberglass tendon glued with resin to the internal barrel surface. Spike anchorages also include (1) the parafil system proposed in Burgoyne (1987) [8] and (2) the split wedge anchorage described in Arnautov et al. (2014) [21].

Split wedge anchorages are composed of (1) an external metallic barrel; (2) two or more internal wedges; and (3) a cable covered by a cylindrical sleeve. They derive from those used to prestress concrete elements and need to be adapted if combined with FRP cables. The wedge shape should be defined [22–26] in order to reduce the bond stress along the FRP cable: this is the purpose of the present work, which will concern the experimental validation of a new anchorage system, after discussing the main literature proposals.

The proposed anchorage is conceived to host one single pultruded carbon cable (ϕ = 12 mm) having a nominal axial capacity of 257 kN. Such an anchorage prototype can be considered a novelty due to the value of the load to be supported that, as far as the kNowledge of the authors is concerned, has been never reached for a one-cable anchorage. On passing, the use of a DIC system to monitor wedge displacements and cable strains can be mentioned as novelty in the framework of the anchorage tests.

2. FRP Tendons

One of the advantages of Fiber-Reinforced Polymer (FRP) composites is their production by tailoring different components that essentially are resins and fibers: additives can be adopted to improve some properties such as fire resistance and durability. Generally, epoxy, vinyl ester, or polyester resins are adopted, combining them with different types of fiber, among which Aramid, Glass, and Carbon can be mentioned: the combination gives rise, respectively, to AFRP, GFRP, and CFRP composite materials.

Those materials have been used to produce several types of ropes, cables, or tendons under the name of Parafil® (AFRP ropes), Polystal® (GFRP tendons), Leadline™ (CFRP tendons), and Carbon Fiber Composite Cable (CFCC), which were the most applied within the civil structural field. Depending on the material mechanical properties and the tendon diameter, the nominal breaking load (P_u) can range between 3.0 and 2500 kN (Table 1).

Table 1. FRP composite tendons: Young's modulus (E), strength (f_u), and breaking load (P_u).

FRP Cable	E (GPa)	f_u (GPa)	d (mm)	P_u (kN)
AFRP Parafil®—Type A	9.8	0.6	3–86	3–2500
AFRP Parafil®—Type F	77.8	1.9	3–39	7.5–1500
AFRP Parafil®—Type G	125.86	1.9	3–39	7.5–1500
AFRP Arapree and FiBRA	65	1.35	-	-
AFRP Technora	54	2.14	-	-
GFRP Polystal®	51	1.5	7.5	66.2
CFRP CFCCs	137	2.12	1.5–5	3.7–41.6
CFRP Leadline™	147	2.55	3–17	18–578.5

Further on, depending on the adopted material, differences are presented in terms of creep (Table 2), environmental and long-term effect (Table 3), stress relaxation (Table 4), and fatigue tests (Table 5).

Table 2. FRP composite tendons: creep properties.

FRP Cable	Creep	Applied Load	Time
AFRP Parafil®—Type A	0.69%/0.41%	0.2 P_u /0.4 P_u	24 h
AFRP Parafil®—Type F	0.09%	Independent	24 h
AFRP Parafil®—Type G	0.036%	Independent	24 h
CFRP CFCCs	0.0073%	0.65 P_u	10^3 h

Table 3. FRP composite tendons: environmental and long-term effect.

FRP Cable	Breaking Load	Applied Load	Time	Environment
AFRP FiBRA	P_u	0.6 P_u	11 months	Alkaline solution
AFRP Technora	P_u	0.58 P_u	200 days	Alkaline solution
AFRP Arapree	0.84 P_u	0.7 P_u	450 days	Alkaline solution
GFRP Polystal®	strength reduction ≈4% due to aging effects strength lower than 30% due to long-term effect			
CFRP CFCCs	P_u	0.5 P_u	375 days	Room temperature
	0.98 P_u	0.7 P_u	104 days	3% sulfuric acid
	0.93 P_u	0.7 P_u	1500 days	NaOH (0.4%) + NaCl (3%)
CFRP Leadline	P_u	-	365 days	NaCl (5%) at 35 °C
	P_u	-	415 days	63 °C

Table 4. FRP composite tendons: relaxation properties.

FRP Cable	Stress Relaxation	Applied Load	Time
AFRP Parafil®—Type G	0.029 P_u /0.045 P_u	0.3 P_u /0.7 P_u	-
AFRP Technora	14%	0.5 P_u	30 days
AFRP FIBRA	12%	0.5 P_u–0.6 P_u	40 days
CFRP CFCCs	0.48%/0.81%/0.96%	0.5 P_u /0.65 P_u /0.8 P_u	100 h

Table 5. FRP composite tendons: fatigue properties.

FRP Cable	Applied Load	Load Range	Cycles to Failure
AFRP Parafil®—Type G	0.30 P_u /0.40 P_u	±0.15 P_u	3.4×10^6/2.9×10^6
AFRP Technora	0.51 P_u	±0.13 P_u	2.0×10^6 without failure
AFRP FiBRA	0.50 P_u	±0.29 P_u	2.0×10^6 without failure
AFRP Arapree	0.40 P_u	±0.15 P_u	2.0×10^6 without failure
GFRP Polystal®	0.50 P_u	±0.034 P_u	3.3×10^7
CFRP CFCCs	0.69 P_u	±0.16 P_u	2×10^6
CFRP Leadline™	0.69 P_u	±0.08 P_u	1×10^6

Based on the collected data, despite the higher cost, carbon FRP cables can be considered the most performing over most material mechanical properties, except for the fatigue performance (Table 5), for which AFRP cables can reach (without failure) a greater number of cycles, but with lower values of the applied load. With this regard, it is worth noticing that investigations on fatigue performance need more attentions, as mentioned in [15].

2.1. Aramid Fiber Tendons

Aramid fiber tendons were produced starting in the early 1960s when Parafil® rope was developed for more navigation platforms: the ropes, made of a bundle of longitudi-

nal dry fibers encased into a protective polymeric sheath, were adopted as prestressing systems [7] and stay cables for footbridges [8]. The main properties are given in [7,27,28] and in the technical notes edited by the producer [29]. Currently, three types of fibers are adopted, having different tensile strength (f_u) and Young's modulus (E): (1) High Tenacity Polyester (Type A, f_u = 0.6, E = 9.8 Gpa), having (a) fiber core nominal diameter (ϕ) ranging between 3 and 86 mm, (b) nominal breaking load (P_u) between 3.0 and 2500 kN; (2) Standard (Type F, Kevlar 29) and High (Type G, Kevlar 49) Modulus Aramid having (a) f_u = 1.9 Gpa and E equal to either 77.8 Gpa (Type F) or 125.86 Gpa (Type G), (b) fiber core nominal diameter ranging between 3 and 39 mm, and (c) nominal breaking load (P_u) between 7.5 and 1500 kN. Creep, stress relaxation, and fatigue tests have been performed. The creep, in the first 24 h was: (1) for Type A, 0.69% and 0.41% respectively at 0.2 and 0.4 P_u; (2) independently on the applied load, equal to 0.09% (Type F) and 0.036 (Type G). Stress relaxation, as far as Type G is concerned, resulted equal to 0.029 P_u (0.09%) and 0.045 P_u (0.06%), having applied an initial load respectively of 0.3 P_u and 0.7 P_u. Fatigue tests were performed on Type G (60 kN) with a load range of $\pm$0.15 P_u (9 kN), resulting 3.4×10^6 and 2.9×10^6 cycles to failure when the mean applied load was equal to 0.30 P_u (18 kN) and 0.40 P_u (24 kN), respectively.

AFRP rods are kNown under the commercial names of Arapree, Technora, and FiBRA for which technical information are collected in [30]. Arapree and FiBRA are based on a combination of epoxy resin, equal to 55 and 35% in volume respectively, and their strength and stiffness are quite similar ($f_u \approx$ 1.35 Gpa, $E \approx$ 65 Gpa). Technora rods ($f_u \approx$ 2.14 Gpa, $E \approx$ 54 Gpa) are composed of vinyl ester resin (35% in volume). Furthermore, useful information concerns creep–rupture, relaxation, environmental resistance, and fatigue. Regarding creep–rupture, it was estimated that Arapree (HM) can respectively sustain (at 20°, for 10^6 h) a load of 0.64 P_u in air and of 0.51 P_u in alkaline solution.

Regarding relaxation: (1) Technora and FiBRA had respectively a value of (a) 14% after 30 days at ≈0.5 P_u and (b) 12% after ≈40 days at 0.5 P_u–0.6 P_u; (2) concerning Arapree, independently of the applied load, after ≈100 years, the predicted values is ≈16% in air and 20% in alkaline solution.

Regarding environmental resistance, the expected values were (1) Arapree: 0.84 P_u after ≈450 days in alkaline solution (pH 13) at 0.7 P_u; (2) Technora: 1.0 P_u in alkaline solution (pH 13) at 0.58 P_u after 200 days; (3) FiBRA: (a) greater than 0.9 P_u after ≈30 days in different solutions (e.g., acid, alkali, artificial sea water, organic solvent), (b) 0.8 P_u in sulfuric acid (H_2SO_4) and (c) 1.0 P_u after 11 months, at 0.6 P_u in alkali solution (pH 13, 60 °C).

Regarding fatigue: (1) Arapree, FiBRA, and Technora can sustain, without failure, 2.0×10^6 cycles, with an alternate load range respectively of 0.4 $\pm$ 0.15 P_u, 0.5 $\pm$ 0.29 P_u, and 0.51 $\pm$ 0.13 P_u. Further useful information on long-term behavior is reported in [31].

2.2. Glass Fiber Tendons

GFRP tendons were introduced in the 1980s, when [32] two West German firms (Bayer AG and Strabag) jointly used the Polystal® to prestress (1) a small bridge (1980) and (2) a two continuous-span bridge (total length ≈ 47 m) for which 19 rods (ϕ = 7.5 mm, V_f = 68%, f_u = 1.5 Gpa, E = 51.0 Gpa), were used for each of the 59 post-tensioned cables. They are characterized by: (1) a strength reduction equal to ≈4% due to aging effects and lower than 30% in case of long-term loading; (2) creeping effects, extrapolated up to a period of 60 years, equal to 3% of the initial elongation; and (3) a limit of 33×10^6 fatigue cycles at 0.5 P_u $\pm$ 0.034 P_u. Further information regard shear strength: (1) it is equal to ≈30 (at 25°) and ≈25 Mpa (70°) in the absence of radial stress, and (2) at 25 °C, it increases almost linearly to 80 Mpa when the radial stress increases between 0 and ≈105 Mpa, showing a coefficient of friction of ≈0.48; (3) at 70 °C, the friction coefficient can be assumed to be ≈0.43 and 0.3 respectively for transversal pressure in between 0–70 and 70–100 Mpa.

2.3. Carbon Fiber Tendons

CFRP tendons date back to the 1990s, when in Japan, CFCC and Leadline™ were respectively developed by Tokyo Rope and Mitsubishi Chemical Corporation, as documented in [30]. CFCC rods (ϕ = 1.5–5 mm) are made of PAN fibers (65% in volume) and epoxy resin. The single strand, even twisted, depending on the number of strands adopted (7, 19, and 37), can have a diameter ranging between 12.5 and 40 mm. The main mechanical properties are: (1) f_u = 2.12 Gpa, E = 137.0 Gpa; (2) residual load at room temperature equal to (a) 1.0 P_u at 0.5 P_u applied for ≈9000 h, (b) 0.98 P_u at 0.7 P_u applied for 2500 h in a 3% sulfuric acid, and (c) 0.93 P_u at 0.7 P_u for 36,000 h in a NaOH (0.4%, pH 13) and NaCl (3.5%) solution; (3) creeping effects was esteemed equal to 0.0073% of the initial elongation if at to 0.65 P_u for 10^3 h; (4) relaxation after 100 h (at 22 °C) was (a) 0.48% at 0.5 P_u, (b) 0.81% at 0.65 P_u, and (c) 0.96% (at 0.8 P_u); (5) 2×10^6 fatigue cycles fatigue cycles were reached with an alternate load ranging between 0.69 ± 0.16 P_u. It is worth noticing that strands (similar to CFCCs) are the NACCs (Nippon steel advanced carbon fiber composite) [10] developed by a consortium of Japanese enterprises (Kajima Corporation, Nippon Steel Corporation, Nippon Steel Chemical Co., Ltd. and Suzuki Metal Industry Co., Ltd.).

Leadline™ pultruded rods (ϕ = 3–17 mm; f_u = 2.55 Gpa; E = 147 Gpa) are composed of pitch-based fibers: (1) no evidence of strength reduction was detected if (a) sprayed at 35 °C with 5% NaCl solution for one year or (b) exposed at 63° for 10^4 h; (2) they sustained up to 10^6 fatigue cycles with an alternate load of 0.69 ± 0.08 P_u.

3. FRP Anchorages

The design of the anchorages strongly depends on the cable required performances: (1) for some applications (e.g., pedestrian cable stayed bridges), the section diameter is defined to minimize deck displacement and vibrations, so that the action load to be transferred is far from the ultimate cable capacity; (2) for other applications (e.g., post tensioning system RC beams), the axial load to be transferred is close to the cable strength, and the efficiency factor (η) is introduced to quantify the anchorage system-to-cable capacity ratio: in [22,25], it is proposed that the value of η should be close to 0.95. However, according to the opinion of the authors, the value of η could be accepted lower than 0.95 when the design is driven by the cable stiffness. So, the cable axial stiffness and nominal failure load are the parameters that characterize the FRP cable as well as the anchorage system, which can be essentially separated into two groups, namely bonded and mechanical anchorages.

The main differences between anchorage types lie in how they transmit forces to the FRP cable surface. Bonded anchorages (Figure 1) are composed of an FRP cable arranged into an external socket, having an internal surface either tapered or not.

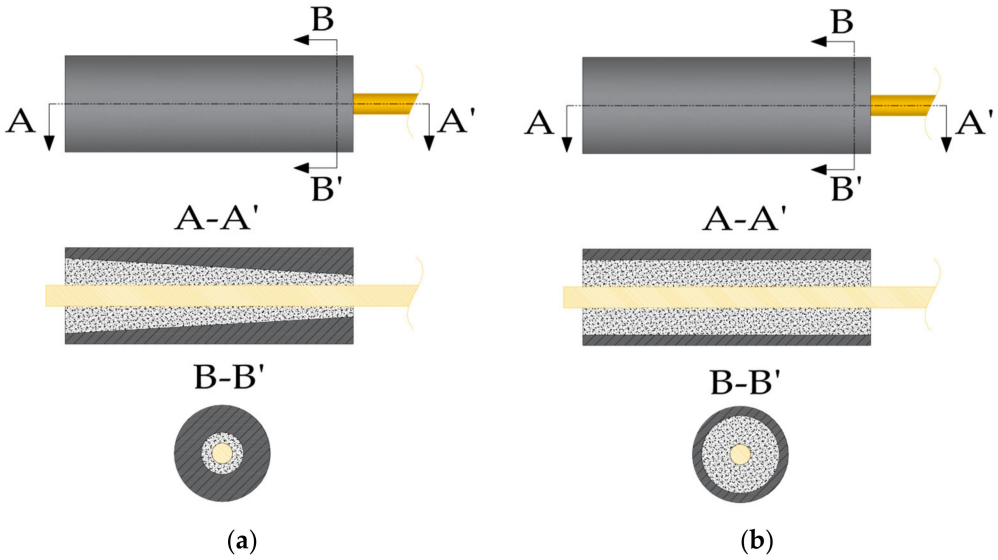

Figure 1. Examples of bonded anchorages with internal surface (**a**) tapered or (**b**) not tapered.

The socket is filled with either resin or mortar. In mechanical anchorages, the FRP cable is kept stuck to the device throughout normal pressure, and the consequent friction, eventually coupled with cohesion, contrasts the applied axial load. Mechanical anchorages can be classified as (a) clamping (Figure 2), (b) spike (Figure 3), and (c) split wedge (Figure 4) systems.

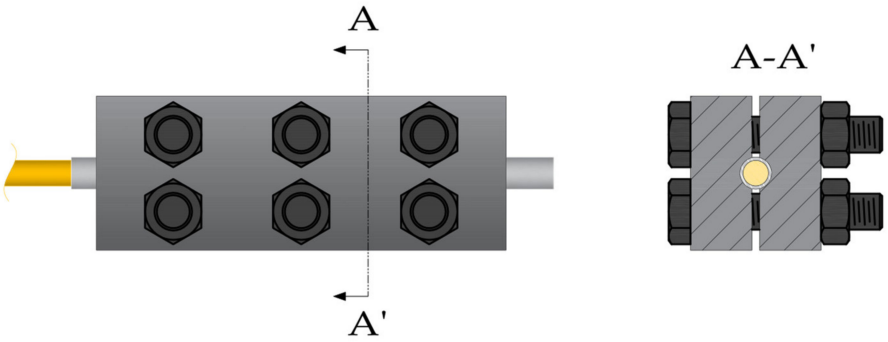

Figure 2. Example of a clamping anchorage composed of two steel plates joined by steel bolts.

Both spike and split wedge anchorages provide a passive pressure once the cable is under tension, whereas the FRP cable is subjected to an active pressure due to a preloading action in clamping anchorages.

Independently of the type of anchorage, the part of cable included in it is generally subjected to axial, shear, and radial stress. The multiple stress state clearly reduces the axial strength of the cable, triggering a premature failure that can be mitigated by (1) adequately protecting the cable with sheaths (denoted as sleeves); (2) adopting adequate potting material in case of bonded anchorages; (3) opportunely tapering (a) the internal surface of the external barrel in case of bonded and split wedge anchorages and (b) the wedge surface in case of split wedge anchorages. The result to be reached is to avoid that the peak values of the single stress (axial, shear, and radial) are not concentrated at the same part of the cable.

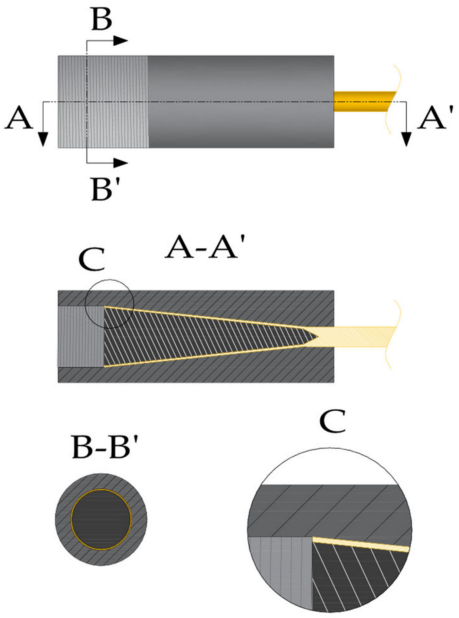

Figure 3. Example of a spike-type anchorage. Detail C magnifies fibers gripped between the conical spike and barrel.

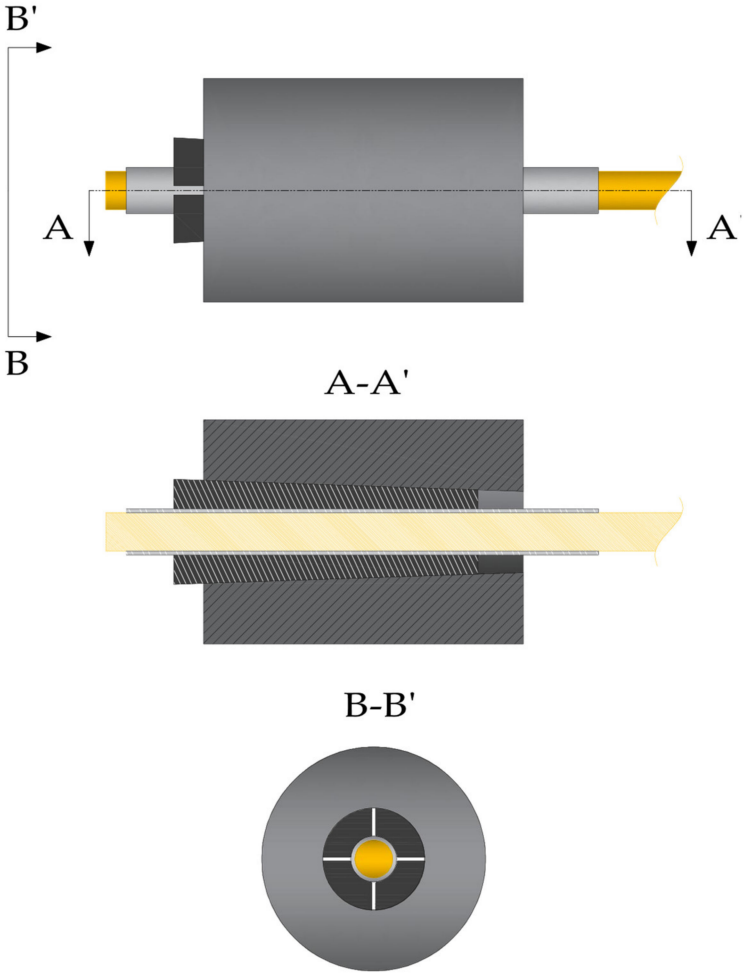

Figure 4. Example of a split wedge anchorage. The FRP cable, protected by a metallic sleeve, is arranged into a tapered barrel together with two or more wedges.

3.1. Bonded Anchorages

Different types of bonded anchorages have been developed, mainly as stay cables. An external CFRP cylindrical socket, filled with expansive mortar, has been adopted for the Tsukuba FRP Bridge (Japan, 1996) [10,13] that is a three-span pedestrian cable-stayed bridge having a total length of 20 m (central span length of 11 m): (1) the GFRP deck is connected to GFRP pylons through 24 CFRP Leadline™ rods (ϕ = 12 mm) and CFCC tendons (ϕ = 15.2 mm) having seven wires (ϕ = 5 mm).

Meier et al. (1998) patented [19] a conical anchor system, proposing a gradient material as anchor body to mitigate shear stress peaks on the cable at the narrowest opening of the socket. The gradient material, named Load Transfer Media (LTM), has a variable density (Figure 5) in order to achieve a Young's Modulus decreasing from the largest to the narrowest part of the conical anchorage, so that (Figure 6) the shear stress distribution is more uniform (Figure 6a) if compared with that (Figure 6b) of a homogeneous potting material.

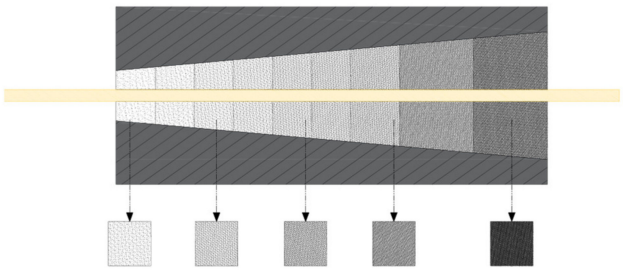

Figure 5. Bonded anchorage filled with Load Transfer Media (LTM). Density of granules gradually decreases from the largest opening to the narrowest end of the socket.

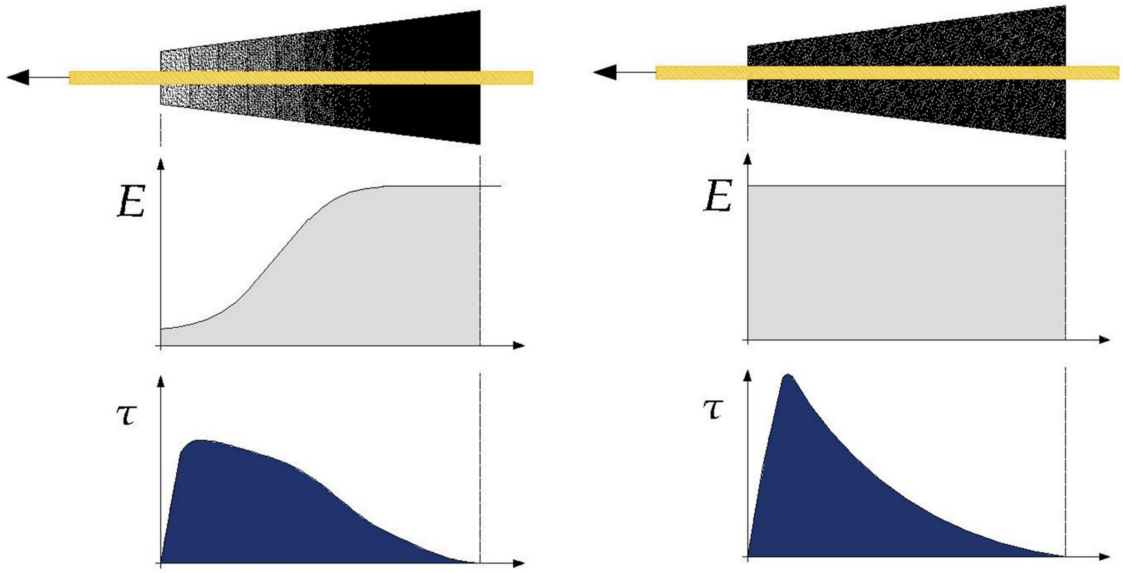

Figure 6. Bonded anchorages with (**a**) and without (**b**) gradient material: distribution of modulus of elasticity (E) and shear stress (τ) at the interface cable-potting materials.

A gradient material was adopted for the Stork Bridge (Switzerland, 1996) [33–35]: (1) the LTM was obtained coating cores (ϕ = 2 mm) of aluminum oxide ceramic with an external epoxy resin; (2) the thickness of the external resin gradually increases from the largest to the narrowest part of the conical anchorage; (3) the cable, composed of 241 wires

(ϕ = 5 mm, f_u = 3.30 and E = 165.0 Gpa), has a global capacity of 12,000 kN; (4) the static capacity of the anchorages is declared to be 92% of the sum of the single wires.

Puigvert et al. (2014) conducted a wide investigation of bonded anchorages potted with epoxy adhesive. They analyzed the static [16], fatigue, and creep [17], as well as stress relaxation behavior [18] of pultruded CFRP cables (ϕ = 8 mm, f_u = 2.50 and E = 140.0 Gpa) bonded into steel tubes with epoxy resin having E = 0.7 Gpa and tensile strength equal to 14.5 Mpa. There were three main conclusions: (1) increasing internal diameter and anchorage length, the static debonding load increases, but the increase is not directly proportional (Table 6); (2) fatigue tests showed that applying an alternate load of 24 $\pm$ 3 kN, the number of sustained cycles is $\approx 1 \times 10^6$; (3) relaxation tests highlighted that, as far as two cases are concerned (ϕ_i = 14 and 18 mm), (a) most of the relaxation occurs after 700 h, (b) for both cases, it was ≈0.40 of the initial applied loads P_0, specifically 21.40 kN = 0.53 P_u (ϕ_i = 14 mm) and 16.78 kN = 0.53 P_u (ϕ_i = 18 mm), (c) increasing the adhesive thickness, a lower initial load is clearly needed to reduce the relaxation (P_0/P_u).

Table 6. Geometry (mm) and ultimate load (kN) of bonded anchorages [16]: (1) Φ_{int} and Φ_{est} = internal and external diameters (mm); (2) L_b = anchorage length.

Properties	Test A	Test B	Test C	Test D
Φ_{int}	14	20	24	14
Φ_{est}	26	26	30	26
L_b	200	200	200	460
P_u	62	75	90	110

3.2. Clamping Anchorages

In clamping anchorages (Figure 2), bolts join the steel plates, which host the FRP cable. Steel plates exert pressure on the cable by tightening bolts, and subsequent friction force ceases the cable from sliding. A crucial aspect, common to all anchorage types, is the limitation of the stress state induced in the cable at the end of the anchorage, where the relative displacements (sliding) are higher. In this critical zone, high values of transversal, longitudinal, and shear stress occur. Other important issues are related to (1) the evaluation of friction coefficient of the sleeve material in contact with the FRP cable; (2) the definition of a strength criterion that takes into account the dependence of shear and axial strength on transversal strength.

Regarding the friction between metallic sleeve and FRP cable, Schön [36] observed that the experimental friction coefficient between aluminum and carbon fiber epoxy composite was ≈0.23, increasing up to 0.68 after imposed loading cycles.

An example of dependence of shear strength on transversal stress has already been introduced as far as GFRP cables are concerned [32]. Moreover, it should be mentioned that [36] the friction coefficient of quasi-isotropic carbon fiber/epoxy material was evaluated ≈0.65, increasing up to 0.74 after imposed loading cycles [37].

3.3. Spike Anchorages

One example of spike anchorage (Figure 3) is the Parafil® tailored for the homonym rope aforementioned [7]: (1) the cable is pushed, through a conical plug, against the internal surface of barrel; (2) the barrel and wedge are usually made aluminum alloy.

Another proposal dates back to 1972, when Davis patented [20] an anchorage for a fiberglass rod (Figure 7); it is essentially composed of (1) an external barrel; (2) a cable inserted in the barrel split in four curved parts; (3) a shaped space-spreader disk with open areas to separate each rod portion; (4) a potting compound of epoxy resin poured through the holes of the space-spreader; (5) a spike made of the same potting material.

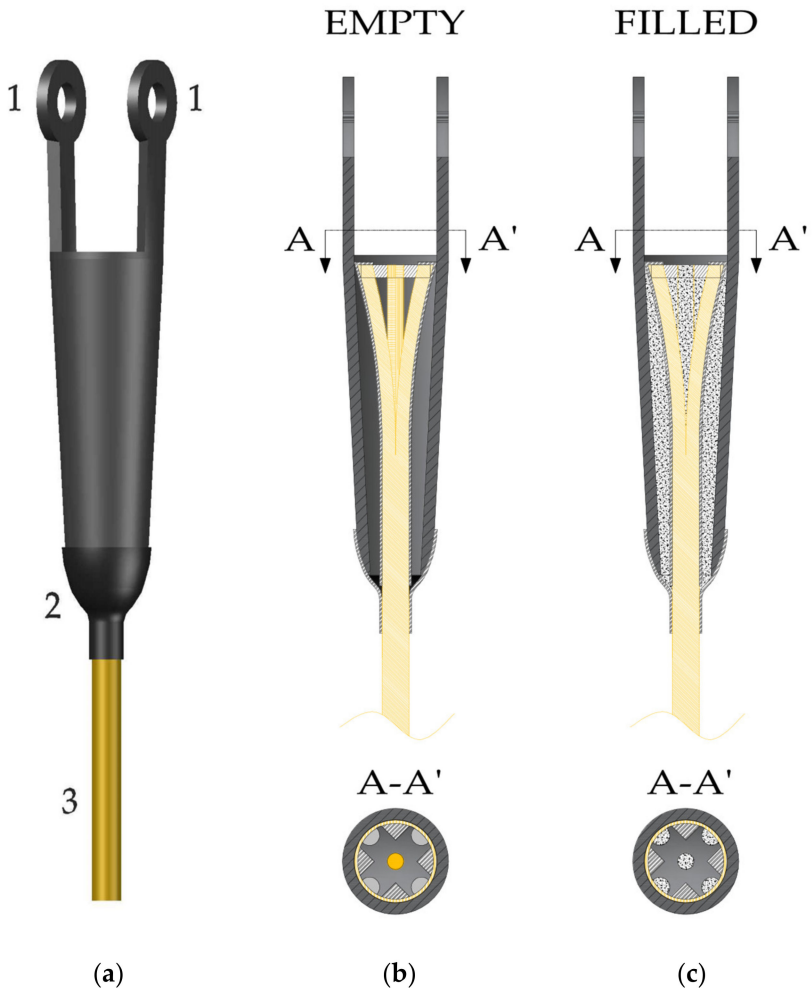

Figure 7. Spike anchorage proposed by Davis [20]: (**a**) 3D representation; (**b**) Four portions of a GFRP cable are first separated by a spacer-spreader; (**c**) Empty spaces are then filled with resin binder. In detail: 1—attaching aligned openings; 2—elastomeric seal; 3—GFRP cable.

A similar solution (Figure 8) was proposed [21] by Arnautov et al. (2014). The tested anchorages were composed of (1) an external steel tube with a thickness of 5 mm having: (a) ϕ_i = 20 mm and L_b = 300 mm when potted with epoxy, (b) ϕ_i = 32 mm and L_b = 500 mm when potted with expanding cement grout; (2) a CFRP rod (ϕ = 5.4 mm and E = 148.0 Gpa), whose split-end has a length of 110 mm; and (3) a conical duralumin wedge (tilted at 7°) glued in the split part of the cable.

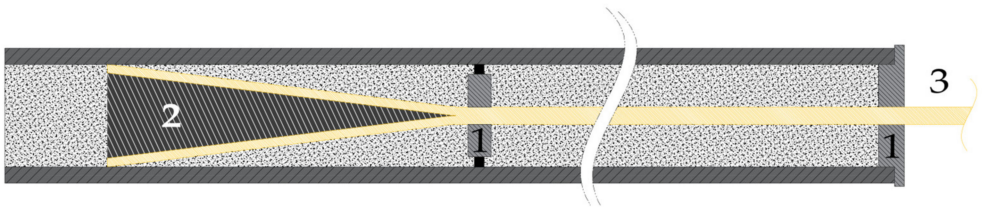

Figure 8. Spike anchorage proposed by Arnautov et al. [21]. In detail: 1—centering rings; 2—duralumin wedges; 3—rod.

Starting from the previous configuration (denoted as full-adhesion contact), two variants have been proposed by treating with polyvinyl alcohol: (1) all the rod surface (full-friction contact) or (2) only the straight part, excluding the wedged part (adhesion-friction contact). Adopting a traditional (not wedged) anchorage (with epoxy), the pull-out force

was ≈29.0 kN. The best performing configurations were those based on epoxy compound, for which results were: (1) full-adhesion (P_u = 46.65 kN); (2) adhesion-friction (P_u = 46 kN); (3) full-friction (P_u = 42.45 kN).

3.4. Split Wedge Anchorages

Split wedge anchorages (Figure 4) are composed of the following: (1) an external metallic barrel, (2) two or more internal wedges, and (3) a core cable covered by a cylindrical sleeve. Their behavior depends on friction forces that act on three contact surfaces, specifically between (1) the cable and the sleeve, (2) the sleeve and the wedges, and (3) the wedges and barrel.

There are two main principles to be observed in order to optimize the morphology: (1) almost null slipping has to occur in between the two inner surfaces (cable-sleeve and sleeve-wedge); (2) the barrel-wedge surfaces should be opportunely shaped in order to minimize their relative displacements (slippage) as well as the radial, tangential, and axial stress in the cable to avoid its premature failure. The barrel-wedge surface is usually shaped, imposing a constant angle between 1° and 15°: the lower the angle, the lower the stress components; however, the slippage is greater. Unconventional solutions, discussed in the following, were presented in [22–25].

Sayed-Ahmed and Shrive (1998) [22] sought to reduce the stress on the cable at the tip of tapered wedges by adopting two different slope angles (Figure 9a) for the internal barrel (1.99°) and the external wedge (2.09°) surfaces [22]; adopting CFRP Leadline™ cables (ϕ = 8 mm), experimental results highlighted the following: (1) failure loads obtained by direct tensile tests, ranging between 105 and 124 kN, were greater than the nominal ultimate load of the cable (P_u = 104 kN); (2) regarding fatigue strength, depending on the scheduled load program, the maximum number of cycles was in between 0.5×10^6 and 2.42×10^6. The highest value was obtained by imposing the following sequence: (1) almost three static cycles (rate = 1kN/s) up to 0.38, 0.58, and 0.86 P_u; (2) 721,000 (5 Hz) cycles between 0.6 and 0.66 P_u; (3) 50 (1 Hz) cycles between 0.5 and 0.8 P_u; (4) almost one static (1 kN/s) test up to 0.9 P_u and (5) 1.7×10^6 (10 Hz) cycles between 0.43 P_u and 0.52 P_u, after which the failure occurred. Further on, FEM analyses have been carried out in order to evaluate the axial, radial, and shear stress along the cable part in contact with the wedge; the results (Figure 9b,c) clearly highlight the following: (a) all the stress components have their peak values at the end part of the contact zone so that (b) the axial strength of the cable is consequently reduced. It is worth noticing that avoiding such stress concentrations was the goal of the system patented by Meier et al. (1998) [19], who proposed a gradient material to reduce the shear peak (Figure 6b), obtaining an almost uniform distribution as reported in Figure 6a.

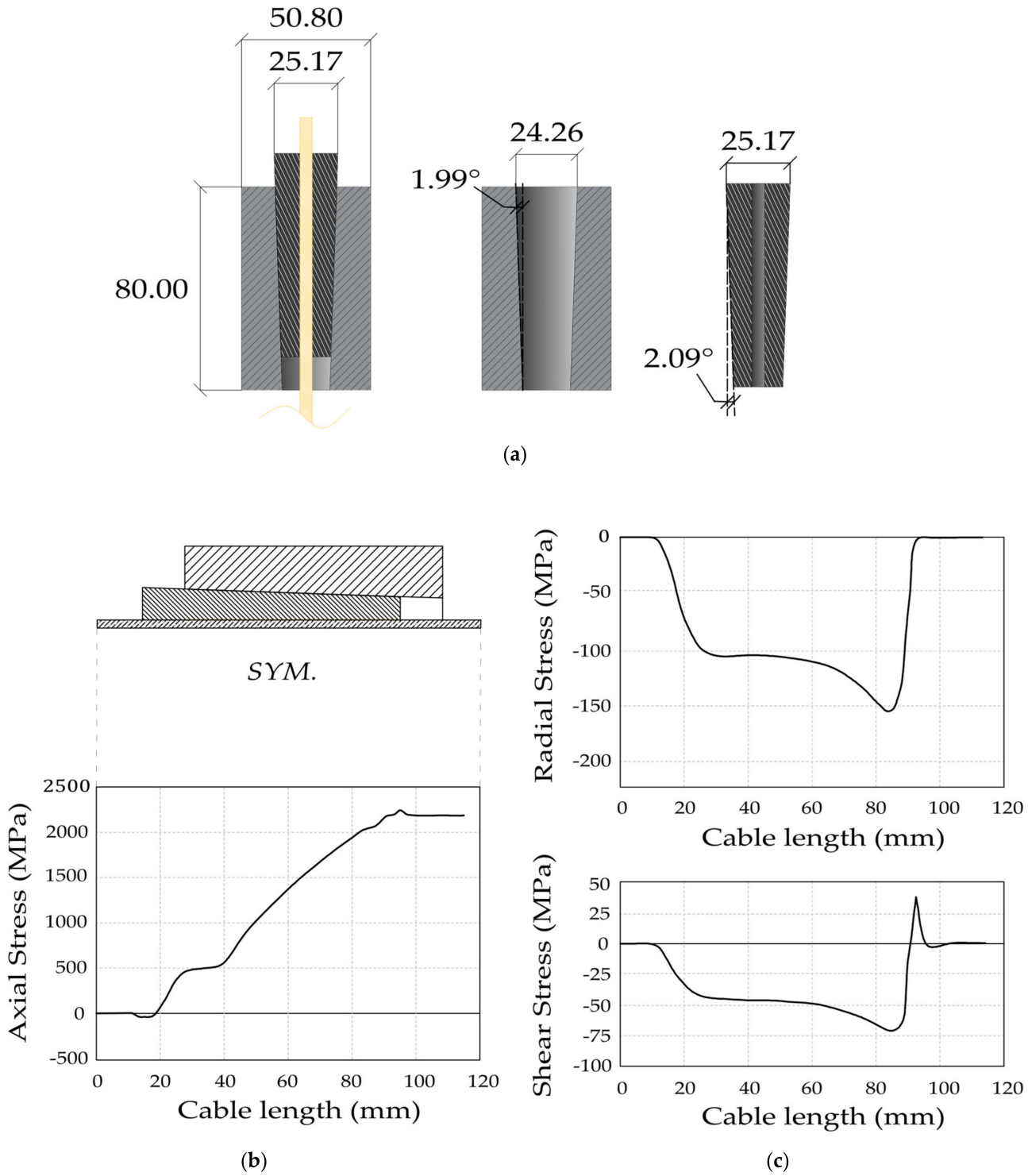

Figure 9. Split wedge anchorage developed by Sayed-Ahmed et al. [22]: (**a**) geometry of the model with differential angle between the barrel and wedges (dimensions in millimeters); (**b**) FEM analyses: longitudinal stress distribution along the cable length; (**c**) FEM analyses–Top: radial stress distribution; Bottom: shear stress distribution. Reproduction of results reported in Sayed-Ahmed et al. [22].

Al-Mayah et al. (2006) proposed [24] a circular curved surface for both the internal and external surfaces of barrel and wedges, respectively (Figure 10): (1) the surfaces have the same curvature radius, which is constant along the height; (2) for both parts, the diameter increases, approaching the free cable end (top part in figure); (3) the internal diameter of the bottom part of the barrel needs to be smaller than the external diameter (b_{wb}) of the bottom

part of the wedge, so that (4) it is kNown the distance (h) between the bottom parts of the two surfaces. The authors tested different barrel/wedge configurations by opportunely varying the radius (R), b_{wb}, and CFRP cable diameter (ϕ = 6.4 mm, P_u = 67 kN; ϕ = 9.4 mm, P_u = 143.5 kN). The conclusions were that (1) no premature failure occurred and (2) by increasing the radius, the relative (barrel/wedge) displacements clearly increased.

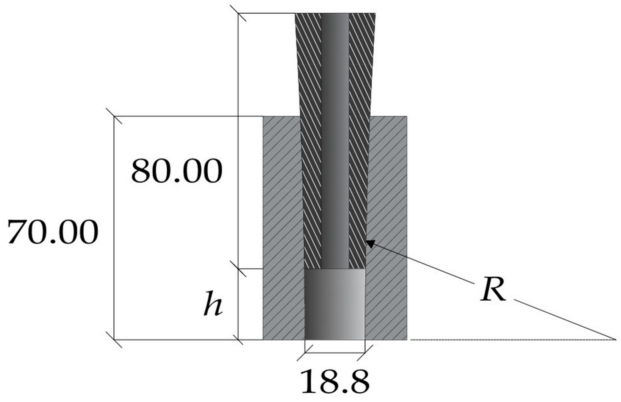

Anchor	R (mm)	b_{wb} (mm)	h (mm)
A	1650	19.1	22.2
B	1763	19.1	23
C	1900	18.95	16.9
D	2100	18.95	17.7

Figure 10. Split wedge anchorage proposed by Al-Mayah et al. [24], with a circular profile between the barrel and wedges. The table reports the adopted values of R, b_{wb}, and h for each anchorage configuration (dimensions in millimeters).

Schmidt et al. (2010) developed [25] an anchorage system for CFRP tendons, where both sleeve and wedges were included into one single element (Figure 11): (1) the barrel inner surface is tilted at 3° with respect to the cable axes; (2) the wedges external surface is tilted at 0.4° with respect to the inner barrel surface; (3) the wedges are connected to each other by two 1 mm thick aluminum walls; (4) only one gap fully separates two adjacent wedges: once the cable is subjected to tensile loads, the sleeve-wedge system starts to slip over the inner barrel surface, and the gap is reduced. Clearly, the one-piece wedge facilitates the optimal settlement during both presetting and loading, as well as the uniform radial stress distribution on the cable. Anchorage specimens were tested, adopting CFRP tendons (ϕ = 8.0 mm, P_u = 120 kN): five tests have been carried out, and the system failure loads ranged between 142 and 149 kN.

Recently, Heydarinouri et al. [26] developed an anchorage that can be considered a combination of the system proposed by (1) Al-Mayah et al. (2006) [24] and (2) Schmidt et al. (2010) [25]. The main peculiarities are represented by (1) circular profiles for a barrel and wedge both made in aluminum; (2) insertion of fillets to the edges of the wedges in contact with the CFRP cable (ϕ = 8.0 mm, P_u = 103 kN); and (3) barrel height and external diameter respectively equal to 80 and 45 mm. Static and fatigue tests have been carried out: (1) the breaking axial load was 16% greater than the cable axial breaking load; (2) no cable failure occurred up to 2.0×10^6 even if (3) for some anchorages, slippage occurred between wedges and cable.

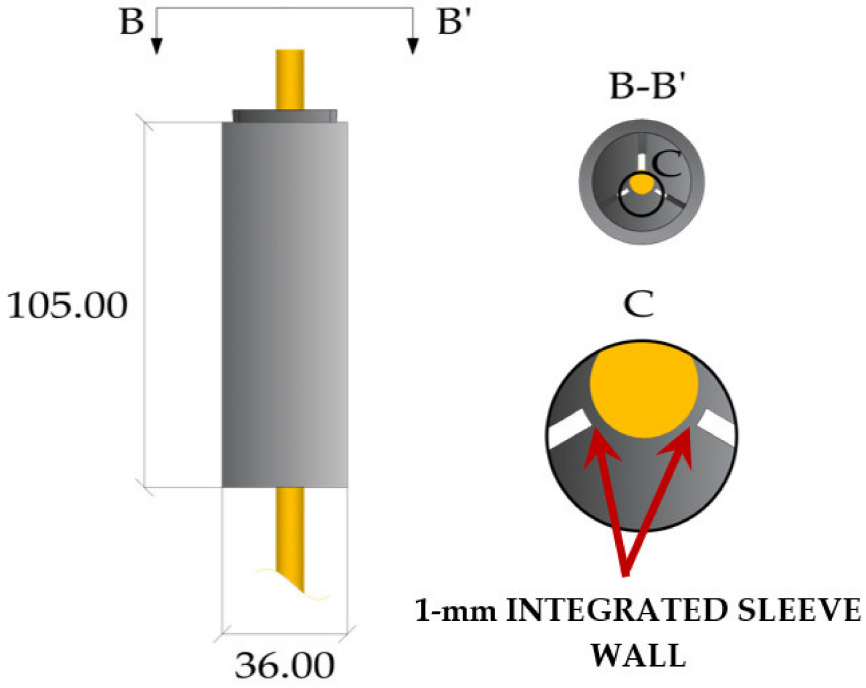

Figure 11. Split wedge anchorage devised by Schmidt et al. [25] with an integrated sleeve (dimensions in millimeters).

4. Proposed Wedge Split Anchorage

Two key problems afflict anchorage design: (1) stress peaks concentration at the narrowest end of the anchorage socket; (2) stabilization of internal slippage between tendon and anchorage.

As far as anchorage for steel (Figure 12) cables is concerned (named traditional in the following), the internal barrel and external wedge angles generally assume higher values than those adopted for FRP cable anchorages. The geometry of an anchorage conceived for a 0.5-inch (≈12 mm) steel cable ($P_u \approx 150$ kN) is reported in Figure 12: (1) the internal barrel surface is inclined by ≈5 degrees; (2) the external surface of the three wedges has a constant slope of 6 degrees; (3) the total height (≈40 mm) is half of the split wedge anchorages for FRP cables discussed in the previous section.

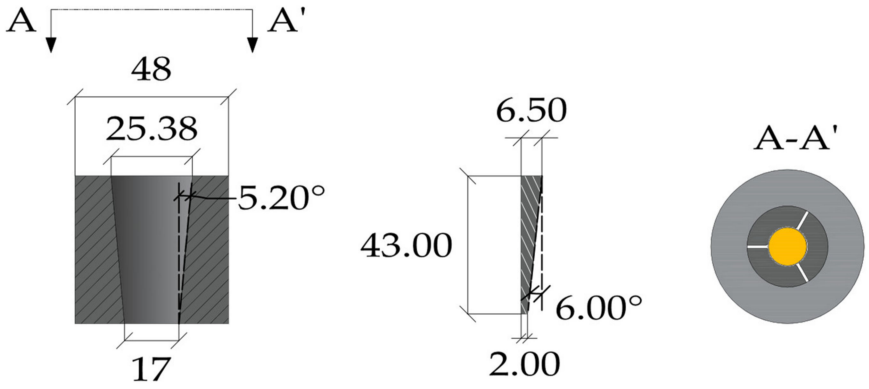

Figure 12. Traditional split wedge anchorage for (ϕ = 12 mm) steel cable: geometry (dimensions in millimeters).

The barrel and wedge of a traditional anchorage have greater slopes than those for FRP cables; it follows that the needed anchorage height is lower, but the stress on the cable increases. So, the geometry of an anchorage conceived for a steel cable with a given

diameter (ϕ) and axial breaking load (P_u) could not be adopted for an FRP cable having the same ϕ and P_u: (1) the slippage between barrel and wedge is almost negligible but (2) the radial and tangential stress assume high values.

As reported in the previous sections, the literature agrees upon the solution of shaping both barrel and wedge contact surfaces in order to mitigate stress concentrations along the FRP cable (see Figure 9b,c). Schmidt et al. (2010) proposed for a 8 mm CFRP tendon (P_u = 120 kN) a differential angle of 0.4° with respect to the inner barrel surface, which is tilted at 3° with respect to the cable axis. The total length of the barrel was 105 mm. Al-Mayah et al. (2006) proposed for a 9.4 mm CFRP cable (P_u = 143.5 kN) a circular-curved shape, with diameter equal to 6.4 (P_u = 67 kN) and 9.4 mm, respectively.

Starting from those solutions, a steel wedge anchorage is proposed for a CFRP tendon (ϕ = 12 mm) having an axial capacity, on average, of 257 kN. As far as the knowledge of the authors is concerned, there are not literature proposals for anchorages that work up that value: as previously introduced, 149 kN [25] was the highest transmitted axial load.

So, the goals of the scheduled work were: (1) preliminary assessment of the performance, in terms of axial capacity, of a traditional wedged anchorage utilizing a CFRP cable; (2) definition of a new barrel and wedge geometry, validating the solution through experimental tests; and (3) implementation of nonlinear finite element analyses in order to assess the influence of principal parameters that include (a) the geometry of the barrel and wedge, (b) mechanical properties of the adopted sleeve, (c) friction coefficient and cohesion of the three contact surfaces between barrel and wedges, wedges and sleeve, and sleeve and cable. Among them, the first two will be discussed in the following sections; whilst detailed FEM studies are in progress, the preliminary results are reported in [38]. Adopted cable, anchorage, and experimental activity will discussed in the following section.

4.1. FRP Cable

The adopted cable is a pultruded CFRP (ϕ = 12 mm) cable: (1) it was manufactured post-treating its external surface through a pull-winding process in order to increase the bond strength; (2) the sleeve consists of two aluminum (E = 70 Gpa) sheaths (1 mm thick) glued with epoxy resin to both ends of the cable.

The material average mechanical properties (E = 164 Gpa; f_u = 2275 Mpa; ε_u = 0.139) have been evaluated by the producer based on five tests (see Table 7) carried out on ϕ = 10 mm tendons, adopting aluminum tabs (700 mm long). The tests have been performed with displacement control at 2 mm/min.

Table 7. CFRP tendon (ϕ = 10 mm): (1) Young's modulus (E_L), (2) strength (f_u), and (3) ultimate strain (ε_u).

Specimen	E (Gpa)	f_u (Mpa)	ε_u (%)
1	163	2375	0.146
2	167	2159	0.129
3	166	2203	0.132
4	161	2256	0.140
5	163	2380	0.146
Average	164	2275	0.139
Standard Deviation	2.44	100	0.0075
Coefficient of Variation	0.015	0.044	0.054

The strain measurements allowed the definition of the Young's secant modulus that, according with [39], (1) refers to the load range of 0.2 P_u–0.5 P_u and (2) needs to be evaluated through an extensometer having a gauge length greater than 100 mm.

Typical failure configurations (Figure 13) denote that there is not a close relation between strength and failure position as well as configuration: (1) specimen 5 had the greater strength (2380 Mpa) but the failure happened close to the anchorage; (2) specimen 2 had the lowest strength (2159 Mpa) even if the break point is not close to the anchorage;

(3) specimen 1, whose strength (2375 Mpa) is close to the highest value, had a configuration that, according with [25], is typical of not premature failure, denoting instantaneous and explosive releases of the stored energy.

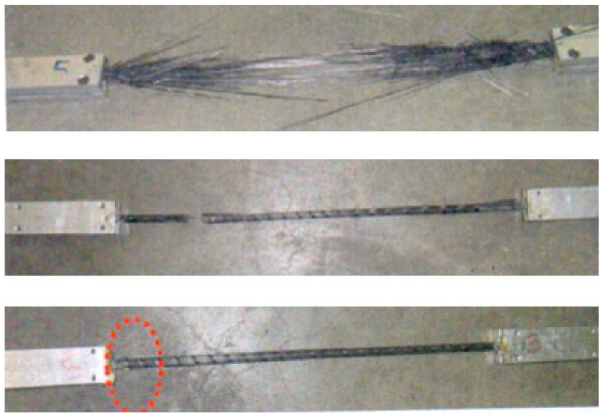

Figure 13. CFRP cable (ϕ = 10 mm)—Typical cable configuration after test: specimen 1 (Up); specimen 2 (Center); specimen 5 (Down).

Based on the properties reported in Table 7, as far as a ϕ = 12 mm cable is concerned, the minimum, maximum, and average value of the breaking load (P_u) are given in Table 8.

Table 8. CFRP tendon (ϕ = 12 mm)—assumed breaking loads (P_u).

Min	Max	Average
244.17	269.17	257

4.2. Anchorage

The proposed anchorage consists of the following (Figure 14): (1) a 100 mm long steel barrel with inner surface tilted at 3° and (2) three steel wedges for which two different solutions have been investigated for the external surface shape having either (a) constant angle (3 degrees) or (b) a 3° angle along the top part, extending for 25 mm, and a 3.1° angle along the remaining part.

Once the geometry was defined, the following single parts of the specimen were produced through a computerized process based on CAD/CAM lathe: (1) two barrels as top and bottom anchorages respectively, (2) 3 + 3 wedges shaped according to the double-angle concept, and (3) 3 + 3 wedges with a constant angle of 3°, that is the angle assumed for the barrel. The two solutions will be denoted as SA (Single Angle) and DA (Double Angle). The adopted steels for barrels and wedges were respectively (1) C45 (E = 220 Gpa; f_y = 395 Mpa; f_u = 649 Mpa) and (2) 16CrNi4Pb (E = 220 Gpa; f_y = 667.8 Mpa; f_u = 694.3 Mpa).

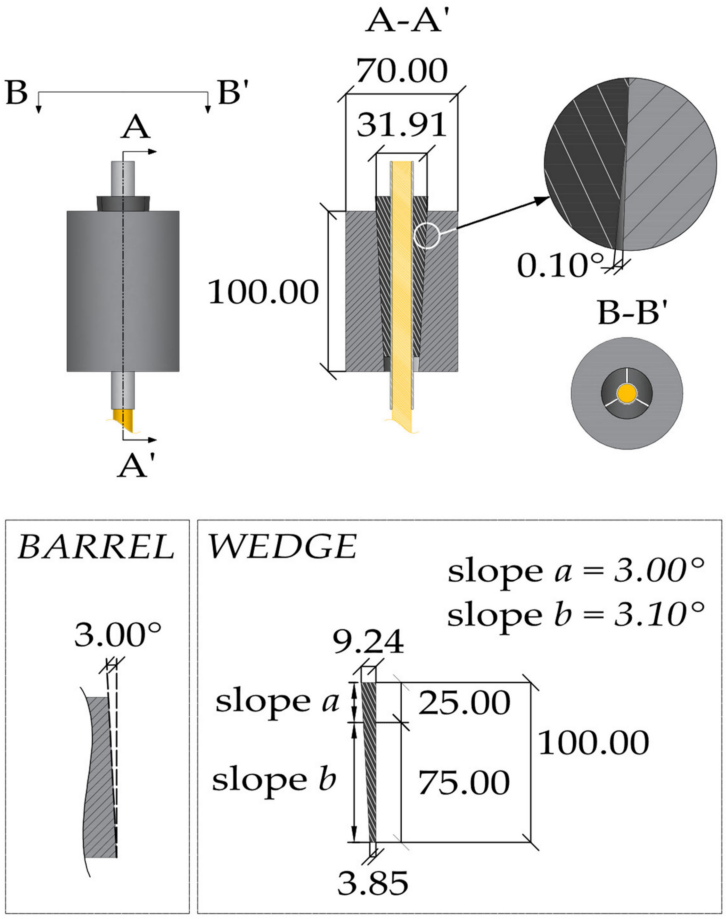

Figure 14. Proposed double-angle wedge anchorage: geometry (dimensions in millimeters).

5. Experimental Campaign

The experimental campaign was performed at the laboratory of Department of Structural and Geotechnical Engineering (Sapienza University of Rome): specimens were tested through an MTS test machine with a displacement control (4 mm/min) and without presetting load.

As far as the traditional anchorage is concerned, force and displacement have been acquired through the MTS system only: the main goal of the test was a preliminary evaluation of the capacity of the anchorage in terms of axial load and displacement, being aware that premature slippage would have occurred.

Regarding the proposed anchorage, for both the SA and DA model, a DIC strategy has been adopted to monitor the field displacements of either the cable surface or the topmost part of the anchorage wedge. These parts of the system have been typically selected by authors [22,24–26] as monitored zones of split wedge anchorages. Clearly, the monitoring systems to be adopted could include (Figure 15 and Table 9): (1) gauges (zones A and B to measure the relative slip between (a) cable and sleeve, (b) sleeve and wedge, (c) wedge and barrel; (2) strain gauges to measure barrel (zone C) and cable (zone E) strain; (3) LVDT between plates D and F: it is worth noticing that the obtained displacements include cable elongation and the aforementioned relative slip.

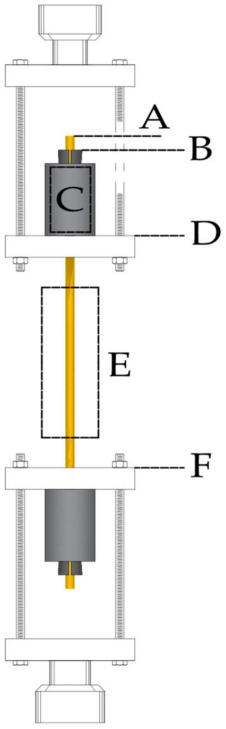

Zone	*Description*
A	Top section of the rod
B	Top section of the wedge
C	Top barrel's outer surface
D	Top section of the upper support
E	Free length of the rod
F	Top section of the lower support

Measuring device		
1	2	3
Displacement transducer (LVDT)	Strain gauge	Digital dial gauge

(**a**) (**b**)

Figure 15. Literature experimental tests on split wedge anchorages—Monitored zones: (**a**) Detail of zones on the anchorage system and a typical test setup; (**b**) Description of the monitored zone and adopted measuring devices.

However, if the system is well designed, barrel external strains are negligible, as well as the relative displacements between (a) cable and sleeve and (b) sleeve and wedges; consequently, only the wedge displacement needs to be monitored for the purpose of the work: this has been done through the DIC system.

Further on, given the limited variability of the Young's modulus (see Table 7) and the almost elastic behavior of the cable, (1) when the axial stress is known, (2) the corresponding strain can be evaluated through the Hook's law and (3) the cable elongation, although negligible if compared with the wedge penetration (slip), can be evaluated assuming a constant axial strain along the cable.

So, (1) a preliminary test has been carried out to monitor displacement and strain field along the cable and to check the negligible slip between (a) the cable and sleeve and (b) the sleeve and wedge; (2) further tests have been monitored controlling the wedge penetration.

The cable monitoring allowed the following at each step: (1) the evaluation of the longitudinal and transversal strain and, consequently, of the Poisson's coefficient; (2) the evaluation of the Young's modulus along the cable, based on the axial stress evaluated dividing the acquired force by the nominal area of the cable: Hook's law has been assumed due to (a) the almost linear elastic behavior of the FRP material as well as (b) its brittle failure; (3) the evaluation of the displacement (d_A) of the central part of the cable (point A in Figure 16) and, consequently, of the displacement of the topmost part of the wedge (part B in Figure 16): the wedge displacement has been evaluated subtracting the cable elongation ($d_A - d_{A'}$) from the global displacement (d_A).

Table 9. Literature experimental tests on split wedge anchorages—monitored zone, adopted measuring device, and measured quantity.

Author	Monitored Zone	Measuring Device	Measured Quantity
Sayed-Ahmed and Shrive [22]	E	Two strain gauges (2)	Strain on the rod's surface
Al-Mayah et al. [24]	A	LVDT (1)	Relative displacement between rod and barrel
Schmidt et al. [25]	C	Six strain gauges (2) along the barrel's height	Circumferential strains along the barrel's height
	E	One strain gauge (2)	Strain on the rod's surface
	B, D, E, F	LVDTs (1)	Wedge penetration and relative displacement between test rig and rod
Heydarinouri et al. [26]	A, B	Digital dial gauge (3)	Displacement of wedges and rod relative to barrel; Wedge seating distance

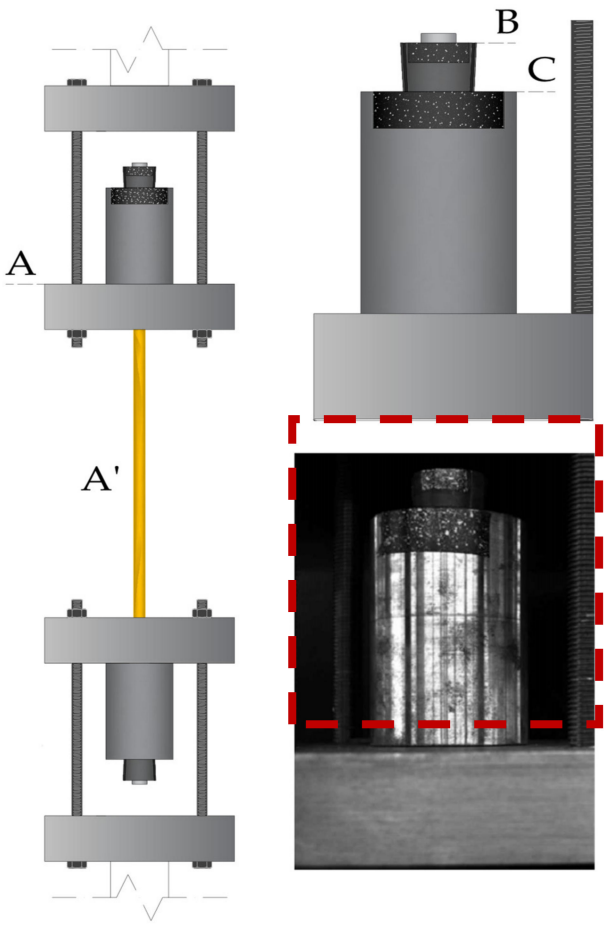

Figure 16. Single and double-angle anchorage—DIC measurement: detail of the monitored parts.

Further tests have been carried out monitoring the wedge displacement of the point B (d_B) and C (d_C) reported in Figure 16 and consequently of the wedge slip ($d_B - d_C$). It is worth noticing that d_C is negligible.

The adopted DIC system consists of the following (Figure 17): (1) one digital camera ("IO Industries" FLARE model) and (2) a digital video recorder ("IO Industries" DVR Express® Core 2 model). The frontal placed camera performed the 2D acquisition: then, data have been elaborated through a software implemented by the authors [40].

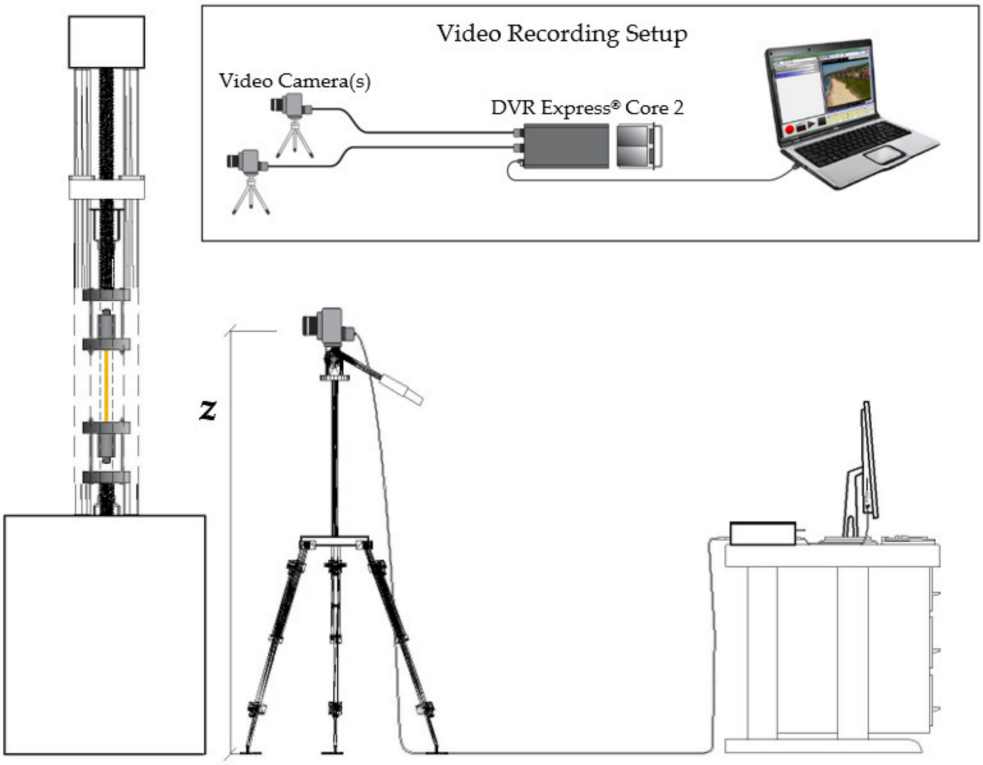

Figure 17. DIC acquiring system.

In order to evaluate cable displacement and strain (Figure 18), (1) the cable images have been discretized by 2 × 12 elements; (2) each element consists of 78 × 74 pixels along the x and y direction, respectively.

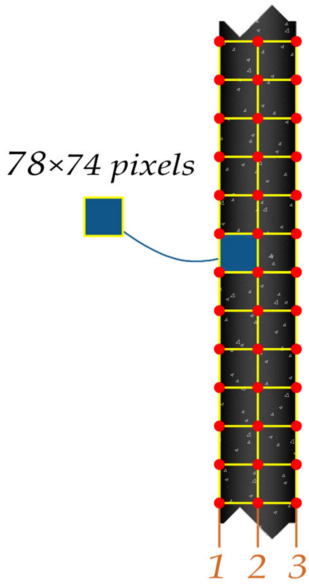

Figure 18. Adopted mesh for DIC analyses: (1) number of pixels within one element and (2) vertical node alignments used to compute the averaged values of strain.

5.1. Traditional Anchorage

The test set up is reported in Figure 19: (1) the CFRP cable and the two anchorages (top and bottom) were encased into two external hollow cylindrical steel supports, to

which the test machine heads are directly screwed; (2) the two barrels were locked through two internal hollow cylinders screwed to the external one. Those internal cylinders were preliminary placed around the cable in between the anchorages.

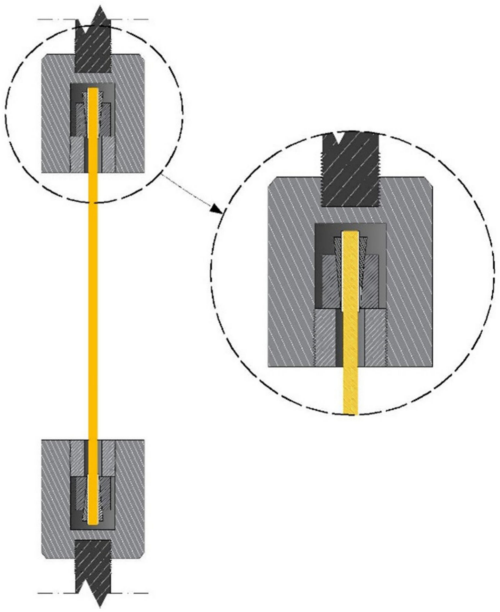

Figure 19. Test setup of the traditional anchorage specimen.

The experimental force–displacement curve (Figure 20) highlights that the premature slippage (between cable and sleeve) occurred at a load of ≈60 kN. Displacements in Figure 20 are those acquired by the testing machine (MTS).

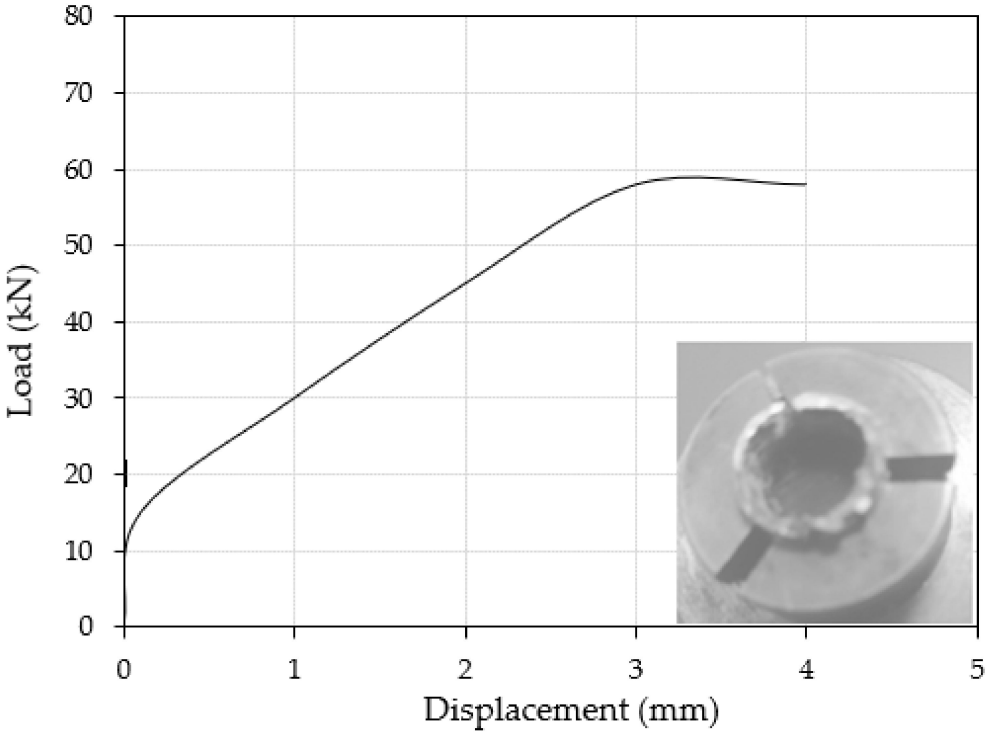

Figure 20. Traditional anchorage: force–displacement curve (MTS results). Evidence of the occurred slip.

5.2. Proposed Anchorage

Experimental tests required the implementation of a specific setup, in order to (1) contrast the predicted pulling action of ≈270 kN, which was (Table 8) the maximum expected axial capacity of the FRP cable, and (2) monitor the wedge through the DIC system. A sketch of the setup is reported in Figure 21 together with (as comparison) the setup adopted for the traditional anchorage: (1) 600 mm long cables have been passed throughout two perforated steel plates (40 mm thick) and then fastened by wedges in the barrels; (2) the plates were connected to the machine through high-strength bolts (ϕ = 16 mm); (3) the load was applied by imposing a vertical displacement of 4 mm/min at the down end of the cable.

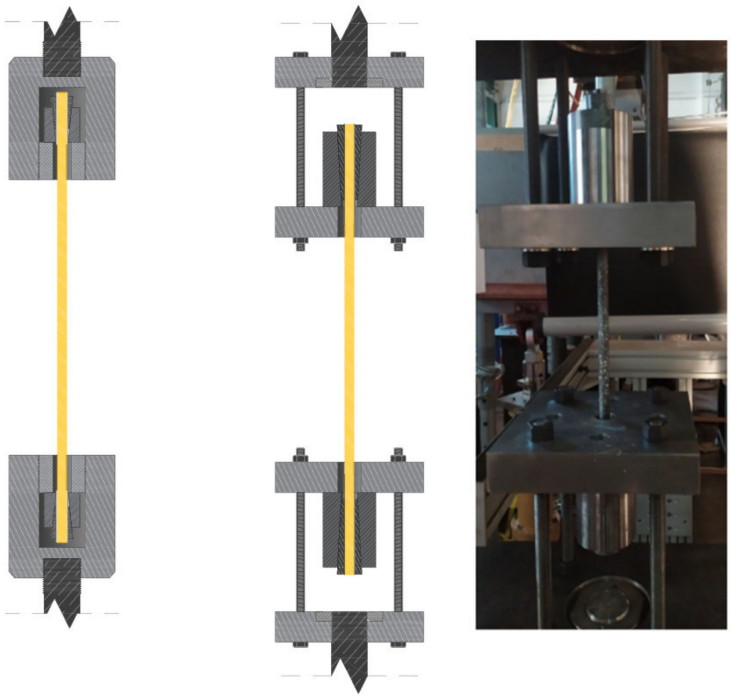

Figure 21. Test setup—Left: traditional anchorage; Right: Single and Double-Angle anchorage (schematic and actual).

Data in terms of force and displacements were also recorded through the MTS acquiring system (see Figure 22), while the DIC system was set to shoot at 10 fps. Three tests for the Single-Angle wedges (SA) and two tests for the Double-Angle wedges (DA) have been carried out. Among them, (1) one SA test was monitored focusing the camera on the cable (zone A in Figure 16); (2) the other four tests were monitored focusing the camera on the topmost part of the wedge (zone BC in Figure 16), which was randomly speckled in order to be tracked by the DIC software.

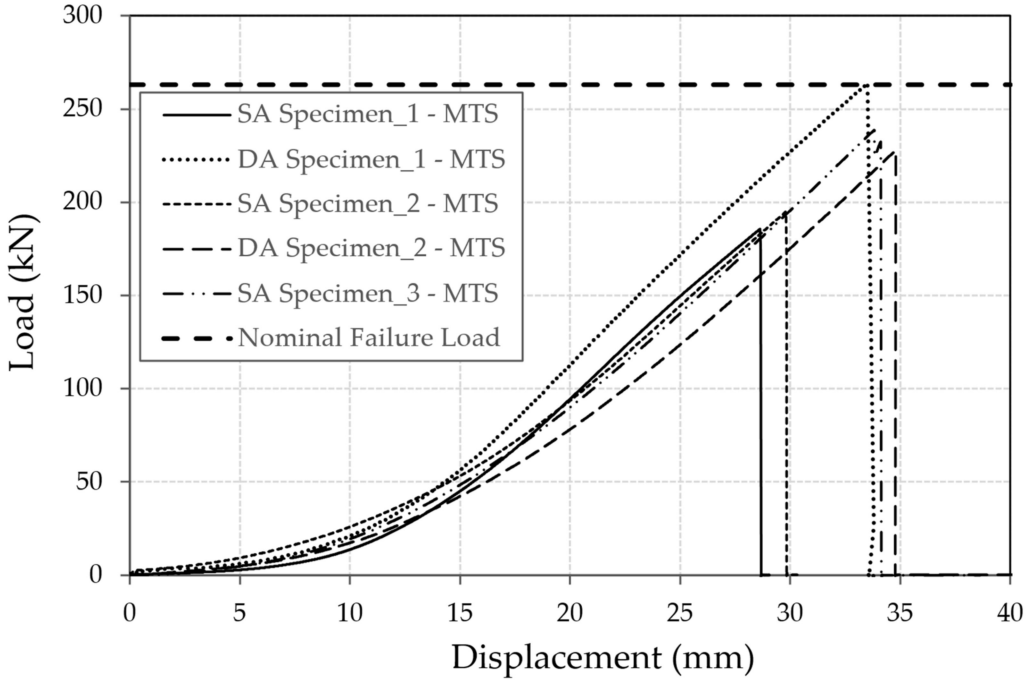

Figure 22. Proposed anchorage: Experimental tests—force–displacement curves (MTS results).

For all the tests, the wedge slip has been evaluated through the procedures previously described: (1) Figure 23a shows an example of the evolution of the wedge configuration at three different levels of force and displacement; (2) Figure 23b includes the force–displacement curves of the whole set of specimens obtained by the DIC system, together with the typical observed rupture that occurred close to the topmost anchorage (Figure 23c).

The results (Table 10) denote the following: (1) the SA wedge system supported a maximum load of 232 kN, but the lower value was equal to 183 kN; (2) the DA wedge system worked up to 222 and 257 kN, so that the higher value (257 kN) is equal to the mean value of the cable strength ($\eta = P_{u\text{-system}}/P_{u\text{-cable}} = 1.0$) and close to the maximum value reported in Table 8.

Table 10. Proposed anchorage: experimental tests. Values of the ultimate load P_u.

Anchorage Model	P_u (kN)
SA Specimen_1	183
SA Specimen_2	194
SA Specimen_3	232
DA Specimen_1	257
DA Specimen_2	222

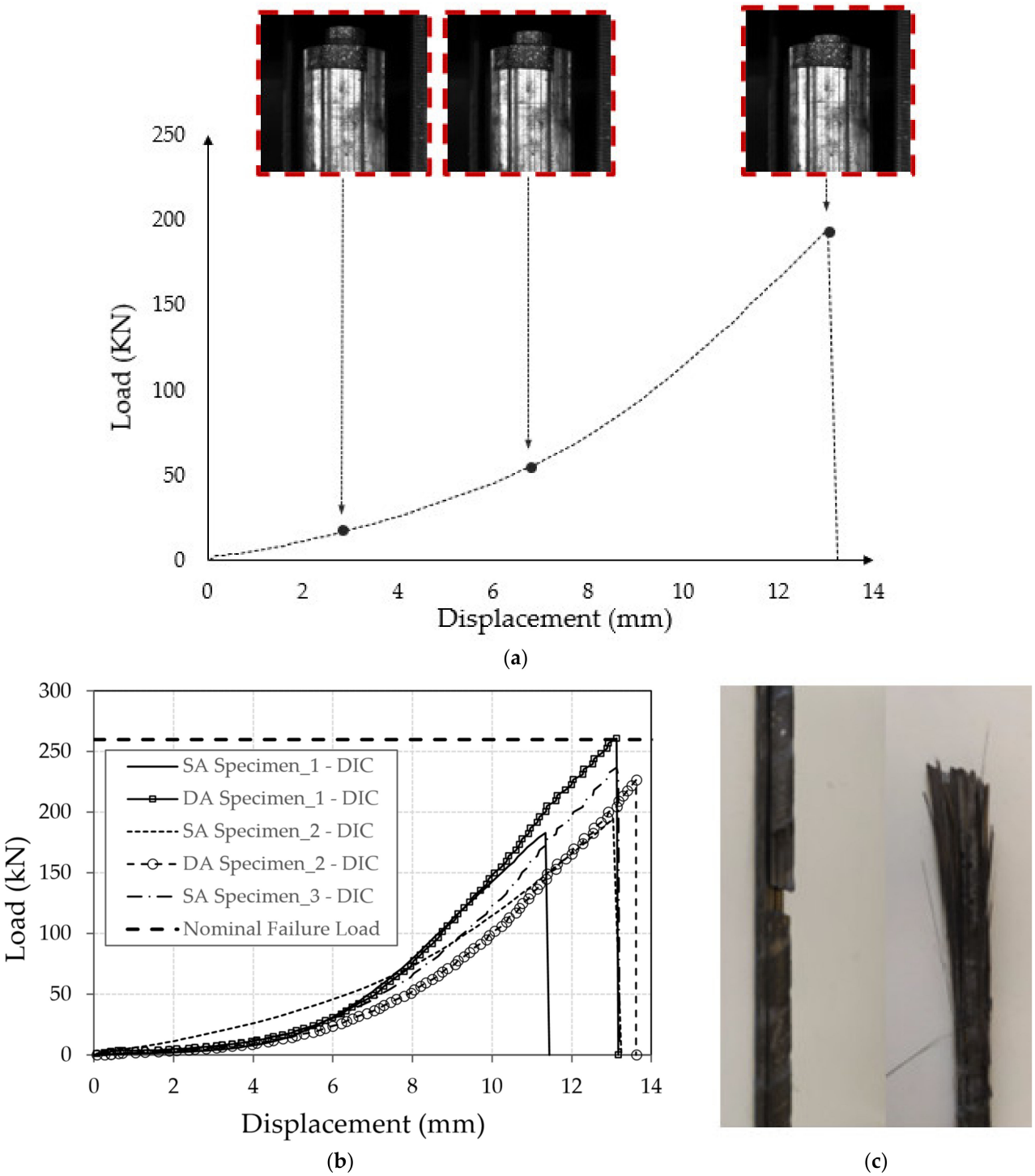

Figure 23. Proposed anchorage–Experimental tests: (**a**) force-displacement curve of the SA specimen_2: evolution of the top wedge displacement at three different levels of force and displacement (DIC results); (**b**) force-displacement curves of specimens (DIC results); (**c**) cable configuration after test (Left: SA_1 and SA_2; Right: DA_1, DA_2, SA_3).

Further on, (1) for higher values of the failure load (DA_1, DA_2, SA_3), a branched configuration can be observed: it denotes a failure that usually happens when the cable capacity is fully (or almost) exploited; (2) for lower values of the failure load (SA_1, SA_2), a shear break could be argued. Rupture in the cable always occurred within the free-length between the two steel plates. Figure 24a shows some frames regarding the SA_2 cable collapse: it can be observed (1) the barrel rocking (Figure 24a) that suggests an

imperfect alignment of the cable; (2) an apparent net tension that afterwards highlighted an internal sliding (Figure 23c) probably triggered by shear consequent to the misalignment. Figure 24b shows the SA_3 cable that, among the SA cables, had the highest breaking load (232 kN): the fiber splitting is usually attributed to a high release of energy and consequently high value of the breaking load.

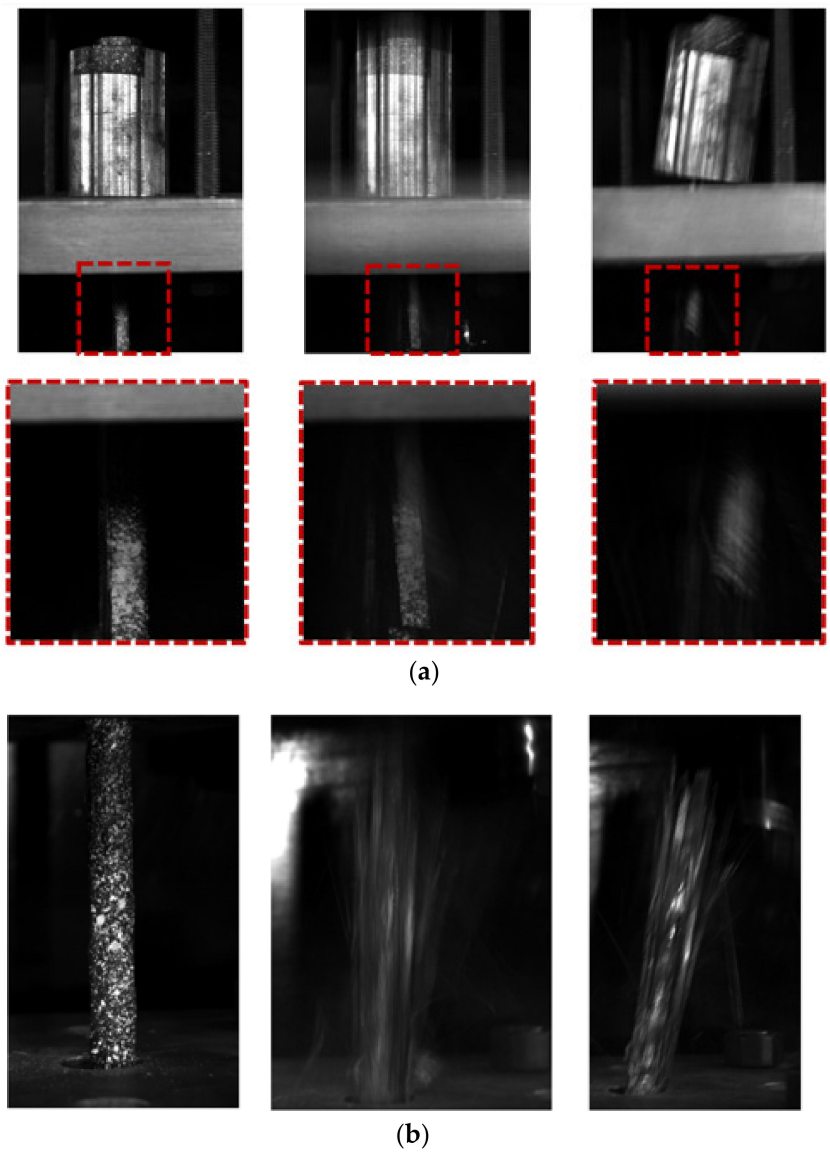

Figure 24. Sequence of frames during the breaking phase: (**a**) SA_Specimen_2–Up: barrel movements; Down: zoom around the breaking zone; (**b**) SA_Specimen_3.

Previous evidence led the authors to conclude that it is not easy to associate the position of the cable rupture with the ultimate load, even because, according to [22], "some cracks tend to extend to (and may be initiated at) the anchorage zone". However, the splitting configurations (Figures 23c and 24b) concern the highest values of P_u.

For one test, the adopted procedure also includes the control of the cable in order to define the strain field on the external surface. Figure 25a shows the mesh selected in the DIC software [40], together with the undeformed and deformed cable configurations. Details on grid dimensions and pixel numbers have been previously reported (see Figure 18). The DIC elaboration allowed the evaluation of the stress–strain curve reported in Figure 25c where axial and lateral strain have been reported. Further on, for three different steps, at 0.2 σ_u, 0.5 σ_u, and σ_u, the longitudinal strain fields have been reported in Figure 25b:

those concerning the steps 0.2 σ_u and 0.5 σ_u have been adopted for the evaluation of the Young's modulus, as recommended in [39]. Axial and lateral strain (Figure 25c) have been evaluated respectively based on the DIC displacement of alignments 2 and 1,3 reported in (Figure 18).

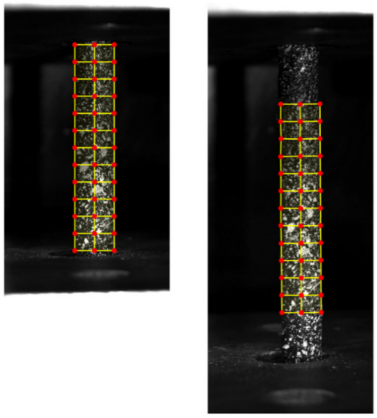

(**a**)

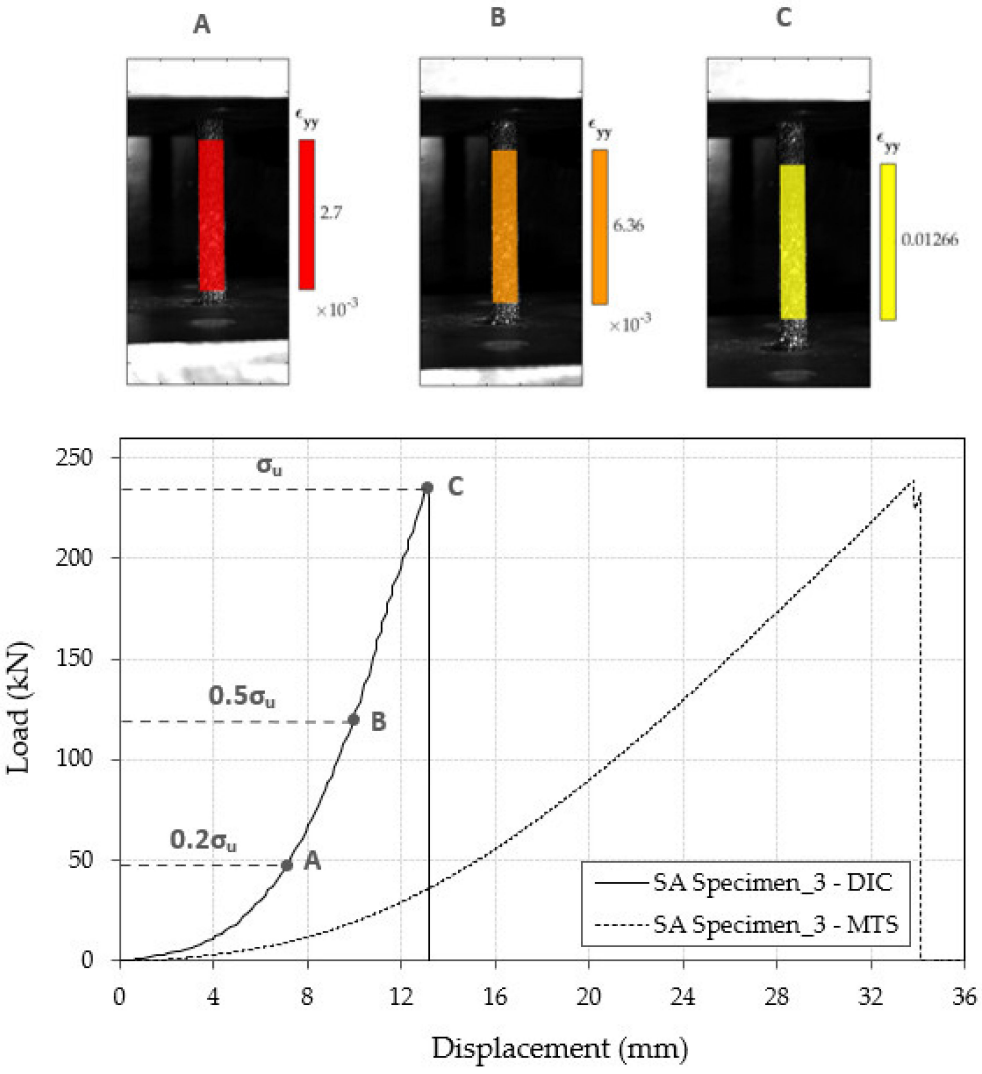

(**b**)

Figure 25. *Cont.*

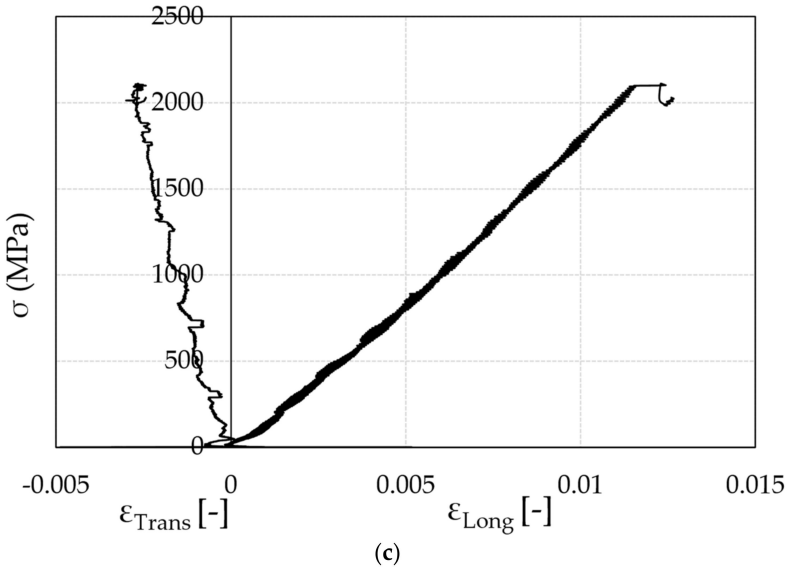

(**c**)

Figure 25. DIC analyses: (**a**) Left: undeformed mesh; Right: deformed mesh relative to a frame close to the cable break; (**b**) SA Specimen_3–Up: longitudinal strain distribution. The reported values have been obtained averaging the strain along the central alignment of the mesh (alignment 2 in Figure 18); (**c**) SA Specimen_3: experimental stress-strain curves (longitudinal –positive– and transversal –negative– strain).

Table 11 shows the obtained values of E_L, ε_u, and ν_{LT}. Comparing the values of E_L and ε_u with those of the producer (Table 7), it follows that the percentage differences respectively are 5.5 and 8.5. However, it is worth noticing that for lower strain values, the DIC results (especially for the Poisson's coefficient) could need higher resolution shooting.

Table 11. Mechanical properties of the CFRP cable: manufacturer (average) vs. DIC values. (1) Longitudinal Young's modulus (E_L); (2) Longitudinal ultimate strain (ε_u) and (3) Longitudinal/transversal Poisson's coefficient (ν_{LT}).

Mechanical Property	Manufacturer Value	DIC Value
ε_u	1.39%	1.27%
E_L	164 Gpa	173 Gpa
ν_{LT} (0.5 σ_u)	N.A.	0.269

6. Conclusions

FRP wires, rods, and tendons offer today the opportunity to approach different materials compared to those traditionally applied in the Civil Engineering field. Even if proposed more than 50 years ago, their application is not widespread: one of the reasons could be a lack of dissemination, among technicians, of the required kNow-how. Many efforts have been devoted to research on different aspects. Some of them have been summarized in this work and regard mechanical properties vs. creep, relaxation, and fatigue, which are properties to be assessed through short-term tests. This implies a difficult correlation with real phenomena in order to predict their durability, even if technical recommendations exist.

FRP rods can be adopted as reinforcement for reinforced concrete elements. Further on, their use as a stay cable and prestressing system is promising if their anchorages are properly designed. Solutions include bonded and mechanical anchorages, which are described in this work before the introduction of a split wedge anchorage. In order to prevent stress peaks at the narrowest end of the barrel, Double-Angle wedges have been proposed and experimentally tested: the system reached a capacity of 257 kN, which is greater than the value obtained in other works. This anchorage can be adopted for an

external FRP cable to improve the capacity of existing reinforced concrete bridge beams subjected to vertical loads.

Further studies are clearly needed, including those concerning fatigue resistance: the existing literature, as far as the kNowledge of the authors is concerned, limits the investigation to $\approx 2.50 \times 10^6$ cycles to failure, which could be inadequate when a high value of yearly heavy traffic occurs.

Author Contributions: (1) Anchorage conceptualization, experimental testing methodology: A.Q.; (2) state of the art, DIC software development and digital image correlation of experimental tests: M.D.; (3) supervision: N.N. All authors have read and agreed to the published version of the manuscript.

Funding: The work has been carried out in the framework of (1) PhD program of the Department of Structural and Geotechnical Engineering (Sapienza University of Rome) and (2) partially in the framework of DPC/ReLUIS project 2019/2021: WP5.4.P2 Task 4: strategies to improve the capacity of existing bridges.

Institutional Review Board Statement: Not applicable.

Informed Consent Statement: Not applicable.

Data Availability Statement: Not applicable.

Conflicts of Interest: The authors declare no conflict of interests.

References

1. Karbhari, V.M.; Seible, F. Fiber reinforced composites—Advanced materials for the renewal of civil infrastructure. *Appl. Compos. Mater.* **2000**, *7*, 95–124. [CrossRef]
2. ACI Committee 440. State-of-the-art report on fiber reinforced plastic (FRP) reinforcement for concrete structures. *Am. Concr. Inst.* **1996**, *96*, 1–68.
3. Japan Society of Civil Engineers. *Recommendation for Design and Construction of Concrete Structures Using Continuous Fiber Reinforcing Materials*; Concrete Engineering Series No. 23; Japan Society of Civil Engineers: Tokio, Japan, 1997.
4. Bank, L.C. Application of FRP Composites to Bridges in the USA. *Proc. Int. Colloq. Appl. FRP Bridg.* **2006**, *1*, 9–16.
5. Bakis, C.E.; Bank, L.C.; Brown, V.L.; Cosenza, E.; Davalos, J.F.; Lesko, J.J.; Machida, A.; Rizkalla, S.H.; Triantafillou, T.C. Fiber-Reinforced Polymer Composites for Construction—State-of-the-Art Review. *J. Compos. Constr.* **2002**, *6*, 73–87. [CrossRef]
6. Einde, L.V.D.; Zhao, L.; Seible, F. Use of FRP composites in civil structural applications. *Constr. Build. Mater.* **2003**, *17*, 389–403. [CrossRef]
7. Hollaway, L. A review of the present and future utilisation of FRP composites in the civil infrastructure with reference to their important in-service properties. *Constr. Build. Mater.* **2010**, *24*, 2419–2445. [CrossRef]
8. Burgoyne, C. Structural use of parafil ropes. *Constr. Build. Mater.* **1987**, *1*, 3–13. [CrossRef]
9. Burgoyne, C.; Head, P. Aberfeldy Bridge—An advanced textile reinforced footbridge. *Techtextil Syposium* **1993**, *418*, 1–9.
10. Karbhari, V.M. *Use of Composite Materials in Civil Infrastructure in Japan*; International Technology Research Institute, Word Technology Research Institute, World technology (WTEC) Division: Baltimore, MD, USA, 1998.
11. ACI Committee 440; American Concrete Institute. Prestressing Concrete Structures with FRP Tendons. 2004. Available online: https://www.iranfrp.ir/wp-content/uploads/2018/12/4404R_04_0.pdf (accessed on 23 March 2021).
12. Schmidt, J.W.; Bennitz, A.; Täljsten, B.; Goltermann, P.; Pedersen, H. Mechanical anchorage of FRP tendons—A literature review. *Constr. Build. Mater.* **2012**, *32*, 110–121. [CrossRef]
13. Liu, Y.; Zwingmann, B.; Schlaich, M. Carbon fiber reinforced polymer for cable structures—A review. *Polymers* **2015**, *7*, 2078–2099. [CrossRef]
14. Wang, L.; Zhang, J.; Xu, J.; Han, Q. Anchorage systems of CFRP cables in cable structures—A review. *Constr. Build. Mater.* **2018**, *160*, 82–99. [CrossRef]
15. Zdanowicz, K.; Kotynia, R.; Marx, S. Prestressing concrete members with fibre-reinforced polymer reinforcement: State of research. *Struct. Concr.* **2019**, *20*, 872–885. [CrossRef]
16. Puigvert, F.; Crocombe, A.D.; Gil, L. Static analysis of adhesively bonded anchorages for CFRP tendons. *Constr. Build. Mater.* **2014**, *61*, 206–215. [CrossRef]
17. Puigvert, F.; Crocombe, A.; Gil, L. Fatigue and creep analyses of adhesively bonded anchorages for CFRP tendons. *Int. J. Adhes. Adhes.* **2014**, *54*, 143–154. [CrossRef]
18. Puigvert, F.; Gil, L.; Escrig, C.; Bernat, E. Stress relaxation analysis of adhesively bonded anchorages for CFRP tendons. *Constr. Build. Mater.* **2014**, *66*, 313–322. [CrossRef]
19. Meier, U.; Meier, H.; Kim, P. Anchorage Device for High-Performance Fiber Composite Cables. U.S. Patent No. 5,713,169, 3 February 1998.
20. Davis, E. Structure for Connecting Attachments to Fiberglass Rods. U.S. Patent No. 3,672,712, 27 June 1972.

21. Arnautov, A.K.; Terrasi, G.P.; Kulakov, V.L.; Portnov, G.G. Fastening of a High-Strength Composite rod with a Splitted and Wedged end in a Potted Anchor 1. Experimental Investigation. *Mech. Compos. Mater.* **2014**, *49*, 595–604. [CrossRef]
22. Sayed-Ahmed, E.Y.; Shrive, N.G. A new steel anchorage system for post-tensioning applications using carbon fibre reinforced plastic tendons. *Can. J. Civ. Eng.* **1998**, *25*, 113–127. [CrossRef]
23. Shrive, N.G.; Sayed-Ahmed, E.Y.; Damson, E.; Tilleman, D.; Tadros, G. Prestressing Anchorage System for Fiber Reinforced Plastic Tendon. U.S. Patent No. 6,082,063, 4 July 2000.
24. Al-Mayah, A.; Soudki, K.; Plumtree, A. Development and Assessment of a New CFRP Rod–Anchor System for Prestressed Concrete. *Appl. Compos. Mater.* **2006**, *13*, 321–334. [CrossRef]
25. Schmidt, J.W.; Bennitz, A.; Täljsten, B.; Pedersen, H. Development of Mechanical Anchor for CFRP Tendons Using Integrated Sleeve. *J. Compos. Constr.* **2010**, *14*, 397–405. [CrossRef]
26. Heydarinouri, H.; Motavalli, M.; Nussbaumer, A. Development of a Mechanical Wedge–Barrel Anchor for CFRP Rods: Static and Fatigue Behaviors. *ASCE J. Compos. Constr.* **2021**, *25*, 04021015. [CrossRef]
27. Burgoyne, C.J. Parafil ropes for prestressing applications. In *Fiber-Reinforced-Plastic (FRP) Reinforcement for Concrete Structures: Properties and Applications*; Nanni, A., Ed.; Elsevier Science Publisher: Amsterdam, The Netherlands, 1993.
28. Burgoyne, C.J. Creep behaviour of a parallel-lay aramid rope. *J. Mater. Sci.* **1992**, *27*, 2473–2489. [CrossRef]
29. Linear Composites Ltd. Parafil—The Ultimate Syntetic Rope—Technical Notes. Available online: www.linearcomposites.com (accessed on 12 March 2021).
30. Benmokrane, B.; Xu, H.; Nishizaki, I. Aramid and carbon fibre-reinforced plastic prestressed ground anchors and their field applications. *Can. J. Civ. Eng.* **1997**, *24*, 968–985. [CrossRef]
31. Saadatmanesh, H.; Tannous, F.E. Long-term behavior of aramid fiber reinforced plastic (AFRP) tendons. *ACI Mater. J.* **1997**, *96*, 297–305.
32. Preis, L.; Bell, T.A. Fiberglass Tendons for Posttensioning Concrete Bridges. *Transp. Res. Rec.* **1987**, *1118*, 77–82.
33. Schurter, U.; Meier, B. Storchen brücke. *Schweiz. Ing. Und Archit. SIA* **1996**. [CrossRef]
34. Meier, H.; Meier, U.; Brönniman, R. Zwei CFK-Kabel für die Storchenbrücke. *Schweiz. Ing. Und Archit. SIA* **1996**, *114*, 8–13.
35. Meier, U. Carbon Fiber Reinforced Polymer Cables: Why? Why Not? What If? *Arab. J. Sci. Eng.* **2012**, *37*, 399–411. [CrossRef]
36. Schön, J. Coefficient of friction for aluminum in contact with a carbon fiber epoxy composite. *Tribol. Int.* **2004**, *37*, 395–404. [CrossRef]
37. Schön, J. Coefficient of friction and wear of a carbon fiber epoxy matrix composite. *Wear* **2004**, *257*, 395–407. [CrossRef]
38. Quadrino, A. FRP Structures. Design of cable stayed pedestrian bridge: Development implementation of an anchorage system. Supervisor: N. Nisticò. Ph.D. Thesis, Sapienza University of Rome, Rome, Italy, 2020.
39. ISO. *Fibre-Reinforced Polymer (FRP) Reinforcement of Concrete—Test Methods—Part 1: FRP Bars and Grids*; International Standard Organization: Geneva, Switzerland, 2008; ISO 10406-1:2008.
40. Damiani, M.; Nisticò, N. Finite element based digital image correlation method. *Intern. Rep.* **2019**, 2–19.